

# Effective One Body description of tidal effects in inspiralling compact binaries

Thibault Damour<sup>1,2</sup> and Alessandro Nagar<sup>1,2</sup>

<sup>1</sup>*Institut des Hautes Etudes Scientifiques, 91440 Bures-sur-Yvette, France*

<sup>2</sup>*ICRANet, 65122 Pescara, Italy*

(Dated: October 23, 2018)

The late part of the gravitational wave signal of binary neutron star inspirals can in principle yield crucial information on the nuclear equation of state via its dependence on relativistic tidal parameters. In the hope of analytically describing the gravitational wave phasing during the late inspiral (essentially up to contact) we propose an extension of the effective one body (EOB) formalism which includes tidal effects. We compare the prediction of this tidal-EOB formalism to recently computed nonconformally flat quasi-equilibrium circular sequences of binary neutron star systems. Our analysis suggests the importance of higher-order (post-Newtonian) corrections to tidal effects, even beyond the first post-Newtonian order, and their tendency to *significantly* increase the “effective tidal polarizability” of neutron stars. We compare the EOB predictions to some recently advocated, nonresummed, post-Newtonian based (“Taylor-T4”) description of the phasing of inspiralling systems. This comparison shows the strong sensitivity of the late-inspiral phasing to the choice of the analytical model, but raises the hope that a sufficiently accurate numerical-relativity–“calibrated” EOB model might give us a reliable handle on the nuclear equation of state.

PACS numbers: 04.25.Nx, 04.30.-w, 04.40.Dg, 95.30.Sf,

## I. INTRODUCTION

Some of the prime targets of the currently operating network of ground-based detectors of gravitational waves (GWs) are the signals emitted by inspiralling and coalescing compact binaries. Here, “compact binary” refers to a binary system made either of two black holes, a black hole and a neutron star, or two neutron stars. The GW signal emitted by binary black hole (BBH) systems has been the subject of intense theoretical studies, based either on analytical methods or on numerical ones. In particular, recent progress in the application of the effective one body (EOB) approach to BBH systems has led to a remarkable agreement between the (analytical) EOB predictions and the best current numerical relativity results [1, 2] (see also [3]). By contrast, much less work has been devoted to the study of the GW signal emitted by compact binaries comprising neutron stars: either black-hole-neutron-star (BHNS) systems or binary neutron-star (BNS) ones. During the inspiral phase (before contact), these systems differ from the BBH ones by the presence of tidal interactions which affect both the dynamics of the inspiral and the emitted waveform. During the merger and coalescence phase, the presence of neutron stars drastically modifies the GW signal [4–6]. The coalescence signal involves (especially in the BNS case) a lot of complicated physics and astrophysics, and is, probably, not amenable to the type of accurate analytical description which worked in the BBH case. Early works on this problem have tried to approximately relate some qualitative features of the merger GW signal linked, e.g., to “tidal disruption”, to analytically describable inputs [7–9].

Recently, Flanagan and Hinderer [10–12] have initiated the program of studying the quantitative influence of tidal effects [11, 13, 14] in inspiralling BNS sys-

tems. However, they only considered the early (lower frequency) portion of the GW inspiral signal, mainly because they were using a post-Newtonian based description of the binary dynamics whose validity is restricted to low enough frequencies. In particular, one of the results of the recent work of Hinderer et al. [12] is to show that the accumulated GW phase due to tidal interactions is, for most realistic NS models of mass  $M \sim 1.4M_{\odot}$  *smaller* than the “uncertainty” in the PN-based description of GW phasing (see the central panel of their Fig. 4 where the thin-dashed and thin-dotted lines are two measures of the PN “uncertainty”. [These measures are larger than the inspiral tidal signal except for the extreme case where the radius of the  $1.4M_{\odot}$  NS is taken to be  $\geq 16$  km].

By contrast, our aim in this work will be to propose a way of describing the binary dynamics (including tidal effects) whose validity does not have the limitations of PN-based descriptions and therefore is not a priori limited to the low frequency part, but extends to significantly higher frequencies. This might be crucial to increase the detectability of the GW signal and thereby have a handle on the nuclear equation of state (EOS). Indeed, our proposal consists in extending the EOB method by incorporating tidal effects in it. Our hope is that such a tidally-extended EOB framework will be able to describe with sufficient approximation not only the early inspiral phase, but also the late inspiral up to the moment (that we shall consistently determine within our scheme) of “contact”. We think that the present EOB description of tidal effects is likely to be more accurate than any of the possible “post-Newtonian-based” descriptions involving supplementary tidal terms (such as [10] or [12]). This should be especially true in the BHNS systems which, in the limiting case  $m_{\text{NS}} \ll m_{\text{BH}}$ , are known to be well described by the EOB approach (and rather badly described by post-Newtonian-based approaches). We will

give some evidence of the validity of the EOB description of close neutron star systems by comparing our analytical predictions to recently calculated quasi-equilibrium neutron star (NS) sequences of circular orbits [15] (see also [16]).

## II. EFFECTIVE-ACTION DESCRIPTION OF TIDAL EFFECTS IN TWO-BODY SYSTEMS

### A. General formalism

The general relativistic tidal properties of neutron stars have been recently studied in Refs. [11–14]. As emphasized in [13], there are (at least) three different types of tidal responses of a neutron star to an external tidal solicitation, which are measured by three different tidal coefficients: (i) a gravito-electric-type coefficient  $G\mu_\ell = [\text{length}]^{2\ell+1}$  measuring the  $\ell^{\text{th}}$ -order mass multipolar moment  $GM_{a_1\dots a_\ell}$  induced in a star by an external  $\ell^{\text{th}}$ -order gravito-electric tidal field  $G_{a_1,\dots,a_\ell}$ ; (ii) a gravito-magnetic-type coefficient  $G\sigma_\ell = [\text{length}]^{2\ell+1}$  measuring the  $\ell^{\text{th}}$  spin multipole moment  $GS_{a_1\dots a_\ell}$  induced in a star by an external  $\ell^{\text{th}}$ -order gravito-magnetic tidal field  $H_{a_1\dots a_\ell}$ ; and (iii) a dimensionless “shape” Love number  $h_\ell$  measuring the distortion of the shape of the surface of a star by an external  $\ell^{\text{th}}$ -order gravito-electric tidal field. It was found in [13, 14] that all those coefficients have a strong sensitivity to the value of the star’s “compactness”  $c \equiv GM/c_0^2 R$  (where we denote by  $c_0$  the velocity of light, to be distinguished from the compactness  $c$ ). This means, in particular, that the numerical values of the tidal coefficients of NS’s should not be evaluated by using Newtonian estimates. Indeed, the dimensionless version of  $\mu_\ell$ , traditionally denoted as  $k_\ell$  (“second Love number”) and defined as

$$2k_\ell \equiv (2\ell - 1)!! \frac{G\mu_\ell}{R^{2\ell+1}}, \quad (1)$$

where  $R$  denotes the areal radius of the NS, is typically three times smaller than its Newtonian counterpart (computed from the same equation of state). A similar, though less drastic, “quenching” also occurs for the “first Love number”  $h_\ell$ . In particular, though Newtonian  $h_\ell$ ’s are larger than 1 (and equal to  $1 + 2k_\ell$ , see Eq. (81) of [13]), the typical relativistic values of  $h_\ell$  are smaller than 1. This will play a useful role in our analysis below of the moment where the tidal distortion of the NS becomes too large for continuing to use an analytical approach.

It was shown in [17, 18] that the motion and radiation of two black holes can be described, up to the fifth post-Newtonian (5PN) approximation, by an effective action of the form

$$S_0 = \int d^D x \frac{\sqrt{g} R(g)}{16\pi G} + S_{\text{point-mass}}, \quad (2)$$

where

$$S_{\text{point-mass}} = - \sum_A \int M_A ds_A, \quad (3)$$

is a “skeletonized” description of black holes, as “point masses”. To give meaning to the addition of point-mass sources to the nonlinear Einstein equations, one needs to use a covariant regularization method. Refs. [17, 18] mainly used Riesz’ analytic regularization, but it was already mentioned at the time that one could equivalently use dimensional regularization. The efficiency and consistency of the latter method was shown by the calculations of the dynamics, and radiation, of BBH systems at the 3PN level [19–21]. Let us also recall that the limitation to the 5PN level in Ref. [18] is precisely linked to the possible appearance of ambiguities in BBH dynamics appearing at the level where tidal effects start entering the picture. Indeed, it is well-known in effective field theory that finite-size effects correspond to augmenting the point-mass action 2 by non-minimal (worldline) couplings involving higher-order derivatives of the field [see [22, 23] and Appendix A of Ref. [24]]. More precisely, the two tidal effects parametrized by  $\mu_\ell$  and  $\sigma_\ell$  correspond to augmenting the leading point-particle effective action, (2), (3), by the following nonminimal worldline couplings

$$\Delta S_{\text{nonminimal}} = \sum_A \left\{ \frac{1}{2} \frac{1}{\ell!} \mu_\ell^A \int ds_A (G_L^A)^2 + \frac{1}{2} \frac{\ell}{\ell+1} \frac{1}{\ell!} \frac{1}{c_0^2} \sigma_\ell^A \int ds_A (H_L^A)^2 \right\}. \quad (4)$$

Here<sup>1</sup>  $G_L^A \equiv G_{a_1\dots a_\ell}^A$  and  $H_L^A \equiv H_{a_1\dots a_\ell}^A$  are the gravito-electric and gravito-magnetic “external” tidal gradients evaluated along the worldline of the considered star (labelled by  $A$ ), in the local frames (attached to body  $A$ ) defined in [25]. If needed, they can be reexpressed in terms of covariant derivatives of the Riemann (or Weyl) tensor. For instance, using Eq. (3.40) of [25], the leading, quadrupolar terms in Eq. (4) read

$$\Delta S_{\text{nonminimal}} = \sum_A \left\{ \frac{1}{4} \mu_2^A \int ds_A \mathcal{E}_{\alpha\beta}^A \mathcal{E}^{A\alpha\beta} + \frac{1}{6} \sigma_2^A \int ds_A \mathcal{B}_{\alpha\beta}^A \mathcal{B}^{A\alpha\beta} + \dots \right\} \quad (5)$$

where  $\mathcal{E}_{\alpha\beta}^A \equiv [u^\mu u^\nu C_{\mu\nu\alpha\beta}]^A$ ,  $\mathcal{B}_{\alpha\beta}^A \equiv [u^\mu u^\nu C_{\mu\nu\alpha\beta}^*]^A$ , with  $C_{\mu\nu\alpha\beta}^* \equiv \frac{1}{2} \epsilon_{\mu\nu\rho\sigma} C_{\alpha\beta}^{\rho\sigma}$  being the dual of the Weyl tensor  $C$ , and  $u^\mu = dz^\mu/ds$  being the four-velocity along the considered worldline. As explained in Appendix A of Ref. [24], one can, modulo some suitable “field redefinitions” that do not affect the leading result, indifferently

<sup>1</sup> We use here the notation of [25], notably for multi-indices  $L \equiv a_1, \dots, a_\ell$ .

use the Weyl tensor  $C_{\alpha\beta\mu\nu}$  or the Riemann tensor  $R_{\alpha\beta\mu\nu}$  in evaluating the  $\mathcal{E}_{\alpha\beta}$  and  $\mathcal{B}_{\alpha\beta}$  entering Eq. (5).

The effective-action terms (4), (5) can be used to compute the various observable effects linked to the relativistic tidal coefficients  $\mu_\ell$  and  $\sigma_\ell$ <sup>2</sup>. In particular, they imply both: (i) additional terms in the dynamics of the considered binary system, and (ii) additional terms in the gravitational radiation emitted by the considered binary system. Both types of additional terms can, in principle, be evaluated with any needed relativistic accuracy from Eq. (4), i.e. computed either in a ‘‘post-Minkowskian’’ (PM) expansion in powers of  $G/c_0^2$ , or (after a further re-expansion in powers of  $1/c_0$ ), in a ‘‘post-Newtonian’’ (PN) expansion in powers of  $1/c_0^2$ . Let us remark in passing that the PM expansion can be conveniently expressed in terms of Feynman-like diagrams, as was explicitly discussed (for tensor-scalar gravity) at the 2PN level in [22].

Here we shall use the extra terms (4), (5) as a way to *add* to the description of binary black hole systems the effects linked to the replacement of one or two of the black holes by a neutron star. From this point of view, we shall conventionally consider that the tidal coefficients of a black hole vanish:  $\mu_\ell^{\text{BH}} = 0 = \sigma_\ell^{\text{BH}}$  [13, 14]. However, as emphasized in [13], more work is needed to clarify whether this is exact, i.e. whether the description of BBH’s by an effective action requires or not the presence of additional couplings of the type of Eqs. (4), (5), as ‘‘counter terms’’ to absorb dimensional regularization poles  $\propto (D-4)^{-1}$  (such poles are indeed linked to the possible ambiguities expected to arise at 5PN in the point-mass dynamics; see the discussion in Sec. 5 of [18]; see also Sec. 7 of [26]). We leave to future work a clarification of this subtle issue.

## B. Leading-Order tidal effects in the two-body interaction Lagrangian

Let us first consider the *dynamical* effects, implied by (4) i.e. the tidal contribution to the ‘‘Fokker’’ Lagrangian describing the dynamics of two compact bodies after having integrated out the gravitational field, say

$$L(\mathbf{q}^A, \mathbf{v}^A) = L^{\text{point-mass}} + L^{\text{tidal}}. \quad (6)$$

Here,  $L^{\text{point-mass}}(q, v)$  denotes the (time-symmetric) interaction Lagrangian following from the point-mass action (2) (say after a suitable redefinition of position variables to eliminate higher derivatives). It is currently

<sup>2</sup> More precisely, Eq. (4) describes only the effects that are *linear* in tidal deformations (and which preserve *parity*). If one wished to also consider *nonlinear* tidal effects one should augment the *quadratic-only* terms (5) by higher-order nonminimal worldline couplings which are cubic, quartic, etc. . . in  $C_{\mu\alpha\nu\beta}$  and its gradients. The coefficients of such terms would then parametrize some *nonlinear* tidal effects, which have not been considered in the linear treatments of Refs. [13, 14].

known at the 3PN level. The supplementary term  $L^{\text{tidal}}$  in Eq. (6) is of the symbolic form (keeping only powers of  $G$  and  $1/c_0$ )

$$\begin{aligned} L^{\text{tidal}} &\sim G^2 \mu_2 \left( 1 + \frac{1}{c_0^2} + G + \dots \right) \\ &+ \frac{G^2 \sigma_2}{c_0^2} \left( 1 + \frac{1}{c_0^2} + G + \dots \right) \\ &+ G^2 \mu_3 \left( 1 + \frac{1}{c_0^2} + G + \dots \right) + \dots \end{aligned} \quad (7)$$

Let us start by discussing the *leading order* contributions associated to each tidal coefficient  $\mu_\ell$  or  $\sigma_\ell$ . The leading term in the contribution linked to  $\mu_\ell$  is simply obtained from (4) by inserting the leading-order value of  $G_L^A$ , i.e. ( $L \equiv a_1 \dots a_\ell$ )

$$G_L^A = [\partial_L U^{\text{ext}}(\mathbf{x})]^A = \partial_L^A \left( \frac{GM^B}{|\mathbf{z}_A - \mathbf{z}_B|} \right) \quad (8)$$

where  $B \neq A$  denotes the companion of body  $A$  in the considered binary system ( $A, B = 1, 2$ ), and  $|\mathbf{z}_A - \mathbf{z}_B|$  the distance between the two bodies. In addition  $\partial_L^A \equiv \partial_{a_1 \dots a_\ell}^A$ , with  $\partial_a^A \equiv \partial/\partial z_A^a$ , denotes the differentiation with respect to  $\mathbf{z}_A$  that appear after taking the limit where the field point  $\mathbf{x}$  tends to  $\mathbf{z}_A$  on the worldline of body  $A$ . Using

$$\partial_L^A \frac{1}{r_{AB}} = (-)^\ell (2\ell - 1)!! \frac{\hat{n}_{AB}^L}{r_{AB}^{\ell+1}} \quad (9)$$

where  $n_{AB}^a \equiv (z_A^a - z_B^a)/r_{AB}$ ,  $r_{AB} \equiv |\mathbf{z}_A - \mathbf{z}_B|$ , and where the hat denotes a symmetric trace-free (STF) projection, and the fact that (see, e.g., Eq. (A25) of [27])

$$\hat{n}_{AB}^L \hat{n}_{AB}^L = \hat{n}_{AB}^L n_{AB}^L = \frac{\ell!}{(2\ell - 1)!!}, \quad (10)$$

one easily finds that the leading Lagrangian contribution proportional to  $\mu_\ell$  reads

$$\begin{aligned} L_{\mu_\ell^A} &= \frac{(2\ell - 1)!!}{2} \mu_\ell^A \frac{(GM^B)^2}{r_{AB}^{2\ell+2}} \\ &= k_\ell^A G(M^B)^2 \frac{R_A^{2\ell+1}}{r_{AB}^{2\ell+2}}. \end{aligned} \quad (11)$$

Here we have used (1) to replace  $G\mu_\ell^A$  in terms of the dimensionless Love number  $k_\ell^A$ , and of the areal radius  $R_A$  of the NS. Note that, in a BNS system, one has to add two different contributions:  $L_{\mu_\ell^A} + L_{\mu_\ell^B}$ . By contrast, in a BHNS system one has only  $L_{\mu_\ell^A}$  if  $A$  denotes the NS.

Let us also evaluate the leading ‘‘magnetic-type’’ contribution, i.e. the term  $\propto \sigma_2$  in (6). It is obtained by inserting in (4) the ‘‘Newtonian’’-level value of the gravitomagnetic quadrupolar field  $H_{ab}^{B/A}$  exerted by body  $B$  on

body  $A$ . This is given by Eq. (6.27a) of [28], namely

$$H_{ab}^{B/A} = -2G \partial_{ac}^A \left( \frac{\epsilon_{abcd} M^B v_{BA}^d}{r_{AB}} \right) - 2G \partial_{bc}^A \left( \frac{\epsilon_{acd} M^B v_{BA}^d}{r_{AB}} \right) \quad (12)$$

where  $v_{BA}^d \equiv v_B^d - v_A^d$  is the relative velocity between  $B$  and  $A$ . A straightforward calculation then yields

$$L_{\sigma_2^A} = 12 \sigma_2^A \frac{(GM^B)^2}{r_{AB}^6} \left[ \left( \frac{\mathbf{v}_{AB}}{c_0} \right)^2 - \left( \frac{\mathbf{n}_{AB} \cdot \mathbf{v}_{AB}}{c_0} \right)^2 \right]. \quad (13)$$

Note that the leading quadrupolar gravito-magnetic contribution (13) is smaller than the corresponding quadrupolar gravito-electric contribution

$$L_{\mu_2^A} = \frac{3}{2} \mu_2^A \frac{(GM^B)^2}{r_{AB}^6} \quad (14)$$

by a factor

$$8 \frac{\sigma_2^A}{\mu_2^A} \left[ \left( \frac{\mathbf{v}_{AB}}{c_0} \right)^2 - \left( \frac{\mathbf{n}_{AB} \cdot \mathbf{v}_{AB}}{c_0} \right)^2 \right]. \quad (15)$$

In terms of the corresponding dimensionless Love numbers  $j_2$  (defined in [13]) and  $k_2$ , the prefactor  $8 \sigma_2^A / \mu_2^A$  is equal to the dimensionless ratio  $j_2 / (4k_2)$ . However, it was found in [13, 14] that the magnetic Love number  $j_2$  was much smaller than  $k_2$ . Typically, for a  $\gamma = 2$   $\mu$ -polytrope and a compactness  $c^A \sim 0.15$ , one has  $j_2 \simeq -0.02$ , while  $k_2 \sim 0.1$ , so that  $8 \sigma_2 / \mu_2 = j_2 / (4k_2) \simeq -0.05$ . In other words, the leading gravito-magnetic interaction (13) is equivalent (say for circular orbits) to a 1PN fractional correction factor,  $1 + \alpha (v_{AB}/c_0)^2$ , modifying the leading gravito-electric contribution (14), with  $\alpha = 8 \sigma_2 / \mu_2 = j_2 / (4k_2) \sim -0.05$ . As we shall discuss below, the 1PN correction to (14), implied by (4), involves coefficients  $\alpha^{1\text{PN}}$  of order unity. We will therefore, in the following, neglect the contribution (13) which represents only a small fractional modification to the 1PN correction to (14). On the other hand, we shall retain some of the higher-degree gravito-electric contributions. Indeed, though, for instance,  $L_{\mu_3^A} \propto 1/r_{AB}^8$  formally corresponds to a 2PN correction to  $L_{\mu_2^A} \propto 1/r_{AB}^6$ , its coefficient is much larger than that corresponding to an order-unity 2PN correction to Eq. (14) [see Table I below].

Summarizing: the leading-order tidal contributions to the two-body interaction Lagrangian are (from Eq. (11))

$$L^{\text{tidal}} = +G \sum_{\ell \geq 2} \left\{ k_\ell^A (M^B)^2 \frac{R_A^{2\ell+1}}{r_{AB}^{2\ell+2}} + k_\ell^B (M^A)^2 \frac{R_B^{2\ell+1}}{r_{AB}^{2\ell+2}} \right\}, \quad (16)$$

where  $k_\ell^A$  denotes the  $\ell^{\text{th}}$  dimensionless Love number of a NS [11, 13, 14]. Note that the plus sign in Eq. (16) expresses the fact that the tidal interactions are *attractive*.

### C. Structure of subleading (post-Newtonian) dynamical tidal effects

Leaving to future work [29] a detailed computation of higher-order relativistic tidal effects, let us indicate their general structure. Here, we shall neglect the effects which are *nonlinear* in the worldline couplings  $\mu_\ell^A$  of Eq. (4) (e.g. effects  $\propto \mu_2^A \mu_2^A$ ) for two reasons. On the one hand, such effects are numerically quite small, even for close neutron stars (as we shall check below). On the other hand, a fully consistent discussion of such effects requires that one considers a more general version of nonminimal worldline couplings, involving terms which are cubic (or more nonlinear) in the curvature tensor and its covariant derivatives. Indeed, it is easily seen that a nonminimal coupling which is *cubic* in  $G_{ab} \sim \mathcal{E}_{\alpha\beta}$  contributes to the dynamics at the same level that a 1PN correction to the coupling quadratic in  $G_{abc}$ .

In the "quadratic-in-curvature" approximation of Eq. (4) the part of the tidal interaction which is proportional to  $\mu_\ell^A$  will have the symbolic structure

$$S_{\mu^A} \sim \mu^A (GM^B)^2 \left[ 1 + GM^A + GM^B + (GM^A + GM^B)^2 + \dots \right] \quad (17)$$

where we only indicate the dependence on  $GM^A$  and  $GM^B$ , leaving out all the coefficients (symbolically replaced by 1), which depend on positions and velocities. The presence of an overall factor  $(GM^B)^2$  comes from the fact that  $G_\ell^A(z^\mu)$  in Eq. (4) (which denotes the *regularized* value of some gradient of the curvature tensor as the field point  $x$  tends to  $z_A^\mu(s_A)$  on the worldline of  $M^A$ ) is proportional to  $GM^B$ , so that it is vanishing when  $M^B \rightarrow 0$ , i.e. in the limit of a one-body system. [We are considering here a two-body system; in the more general case of an  $N$ -body system we would have  $G^A(z_A) \propto \sum_{B \neq A} GM^B$ .] In a diagrammatic language (see e.g. [22]) the higher-order terms on the right hand side (r.h.s.) of Eq. (17) correspond to diagrams where, besides having the basic (quadratic in  $h_{\mu\nu}$ ) vertex  $\mu_A$  on the  $A$  worldline being connected by two gravity propagators to two  $GM_B$  "sources" on the  $B$  worldline, we also have some further gravity propagators connecting one of the worldlines either to one of the worldline vertices, or to some intermediate "field" vertex. Note that the information about the 1PN corrections to both gravito-electric ( $\mu_\ell$ ) and gravito-magnetic ( $\sigma_\ell$ ) multipolar interactions (of any degree  $\ell$ ) is contained in the work of Damour, Soffel and Xu [28, 30, 31]. We shall discuss below the effect of the subleading (post-Newtonian) terms in (17) on the EOB description of the dynamics of tidally interacting binary systems.

### III. INCORPORATING DYNAMICAL TIDAL EFFECTS IN THE EFFECTIVE ONE-BODY (EOB) FORMALISM

#### A. General proposal

The EOB formalism [32–34] replaces the two-body interaction Lagrangian (or Hamiltonian) by a Hamiltonian, of a specific form, which depends only on the relative position and momentum of the binary system, say  $(\mathbf{q}, \mathbf{p})$ . For a non spinning BBH system, it has been shown that its dynamics, up to the 3PN level, can be described by the following EOB Hamiltonian (in polar coordinates, within the plane of the motion):

$$H_{\text{EOB}}(r, p_{r_*}, p_\varphi) = M\sqrt{1 + 2\nu(\hat{H}_{\text{eff}} - 1)} \quad (18)$$

where

$$\hat{H}_{\text{eff}} = \sqrt{p_{r_*}^2 + A(r)} \left( 1 + \frac{p_\varphi^2}{r^2} + z_3 \frac{p_{r_*}^4}{r^2} \right). \quad (19)$$

Here  $M = M_A + M_B$  is the total mass,  $\nu \equiv M_A M_B / (M_A + M_B)^2$  is the symmetric mass ratio and  $z_3 \equiv 2\nu(4 - 3\nu)$ . In addition we are using rescaled dimensionless (effective) variables, notably  $r = r_{AB}/GM$  and  $p_\varphi = P_\varphi / (GM_A M_B)$ , and  $p_{r_*}$  is canonically conjugated to a “tortoise” modification of  $r$  [36].

A remarkable feature of the EOB formalism is that the complicated, original 3PN Hamiltonian (which contains many corrections to the basic Newtonian Hamiltonian  $\frac{1}{2}\mathbf{p}^2 + 1/r$ ) can be replaced by the simple structure (18), (19) whose two crucial ingredients are: (i) a “double square-root” structure  $H_{\text{EOB}} \sim \sqrt{1 + \sqrt{\mathbf{p}^2 + \dots}}$ , and (ii) the “condensation” of most of the nonlinear relativistic gravitational interactions in one function of the (EOB) radial variable: the basic “radial potential”  $A(r)$ . In addition, the structure of the function  $A(r)$  is quite simple. At the 3PN level it is simply equal to

$$A^{3\text{PN}}(r) = 1 - 2u + 2\nu u^3 + a_4 \nu u^4, \quad (20)$$

where  $a_4 = 94/3 - (41/32)\pi^2$ , and  $u \equiv 1/r = GM/r_{AB}$ . It was recently found [1] that an excellent description of the dynamics of BBH systems is obtained by: (i) augmenting the presently computed terms in the PN expansion (20) by additional 4PN and 5PN terms, and by (ii) Padé-resumming the corresponding 5PN “Taylor” expansion of the  $A$  function. In other words, BBH (or “point mass”) dynamics is well described by a function of the form

$$A^0(r) = P_5^1 [1 - 2u + 2\nu u^3 + a_4 \nu u^4 + a_5 \nu u^5 + a_6 \nu u^6], \quad (21)$$

where  $P_m^n$  denotes an  $(n, m)$  Padé approximant. It was found in Ref. [1] that a good agreement between EOB and numerical relativity binary black hole waveforms is obtained in an extended “banana-like” region in

the  $(a_5, a_6)$  plane approximately extending between the points  $(a_5, a_6) = (0, -20)$  and  $(a_5, a_6) = (-36, +520)$ . In this work we shall select the values  $a_5 = -6.37$ ,  $a_6 = +50$  which lie within this good region.

Our proposal for incorporating dynamical tidal effects in the EOB formalism consists in preserving the simple general structure (18), (19) of the EOB Hamiltonian, but to modify the BBH radial potential (21) (which corresponds to the point-mass action (2)) by augmenting it by some “tidal contribution”. In other words the proposal is to use Eqs. (18), (19) with

$$A(r) = A^0(r) + A^{\text{tidal}}(r). \quad (22)$$

#### B. Incorporating leading order (LO) dynamical tidal interactions

Let us show that, at the leading order (LO), one can use a tidal contribution of the form

$$A_{LO}^{\text{tidal}}(r) = - \sum_{\ell \geq 2} \kappa_\ell^T u^{2\ell+2}, \quad (23)$$

with some dimensionless coefficient  $\kappa_\ell^T$ .

Indeed, if we keep only the Newtonian approximation of the full EOB Hamiltonian (18), (19) (using  $A(r) \equiv 1 + \bar{A}(r)$  with  $\bar{A}(r) = -2GM/(c_0^2 r_{AB}) + \dots$  being 1PN small as  $1/c_0^2 \rightarrow 0$ ) one finds (with  $\mu \equiv M^A M^B / M$ )

$$H_{\text{EOB}} \simeq M c_0^2 + \frac{1}{2} \mu \mathbf{p}^2 + \frac{1}{2} \mu \bar{A}(r) + \mathcal{O}\left(\frac{1}{c_0^2}\right), \quad (24)$$

which exhibits the role of  $\frac{1}{2} \mu \bar{A}(r)$  as being the interaction energy. Decomposing  $\bar{A}(r) = \bar{A}^0(r) + A^{\text{tidal}}(r)$ , and remembering that there is a sign reversal between the interaction energy and the interaction Lagrangian, we see that the terms (16) can be converted in a contribution to the  $A(r)$  potential of the form (23), if the coefficients  $\kappa_\ell^T$  take the values

$$\begin{aligned} \kappa_\ell^T &= 2 k_\ell^A \frac{M_B}{M_A} \left( \frac{R_A c_0^2}{G(M_A + M_B)} \right)^{2\ell+1} \\ &\quad + 2 k_\ell^B \frac{M_A}{M_B} \left( \frac{R_B c_0^2}{G(M_A + M_B)} \right)^{2\ell+1} \\ &= 2 \frac{M_B M_A^{2\ell}}{(M_A + M_B)^{2\ell+1}} \frac{k_\ell^A}{c_A^{2\ell+1}} \\ &\quad + 2 \frac{M_A M_B^{2\ell}}{(M_A + M_B)^{2\ell+1}} \frac{k_\ell^B}{c_B^{2\ell+1}}. \end{aligned} \quad (25)$$

In the second form, we have introduced the compactness parameters of the stars:  $c_A \equiv GM_A/(R_A c_0^2)$ . It is interesting to note that the dimensionless tidal parameters that enter the EOB dynamics are (when  $M_A \sim M_B$ ) the ratios  $k_\ell^A/c_A^{2\ell+1}$ , rather than the Love numbers  $k_\ell^A$ . Let us also note that the velocity of light  $c_0$  formally appears in the numerator of  $\kappa_\ell^T$ . This is related to the fact that, contrary to the coefficients of the successive powers of  $u$  that

TABLE I: Tidal properties of BNS and BHNS system. The NS model is obtained using the piece-wise polytropic representation of EOS SLy and has compactness  $c = 0.17385$ . Other properties of the model can be found in Table II.

Model	$q$	$\kappa_2^T$	$\kappa_3^T$	$\kappa_3^T$
BNS	1	73.0426	165.2966	509.6131
BHNS	4	1.4959	0.5416	0.2672
BHNS	10	0.0726	0.0054	0.0005

enter the BBH EOB potential  $A^0(r)$  which are (roughly speaking) pure numbers of order unity, the coefficients  $\kappa_\ell^T$  entering the tidal contribution  $A^{\text{tidal}}(r)$  will tend to be much larger than unity (and to increase with  $\ell$ ). For instance, we shall typically find that  $\kappa_2^T = \mathcal{O}(100)$ . This numerical difference makes it consistent to add to  $A^0(r)$  (which is known for sure only up to  $u^4$  terms, i.e. the 3PN level) additional terms  $\propto u^6 + u^8 + \dots$  that would formally correspond to 5PN + 7PN +  $\dots$  contributions if their coefficients were “of order unity” (at least in the parametric sense).

Finally, to illustrate the typical numerical values of the EOB tidal parameters we give in Table I the values of  $\kappa_2^T$  for three paradigmatic systems, one equal-mass BNS and two BHNS of mass ratios  $q \equiv M_{BH}/M_{NS} = 4$  and  $q = 10$ . The neutron star model is described with a “realistic” EOS SLy (with a piece-wise polytropic representation, see below) and has the following characteristics: mass  $M = 1.35M_\odot$ , compactness  $c = 0.17385$ , radius  $R = 11.466$  km. Note that the main dependence on the equation of state (EOS) in  $\kappa_\ell^T$  (say for the equal-mass BNS case) comes from  $\kappa_\ell^T \propto R_A^{2\ell+1}$ . Therefore, if one were considering a NS of different radius (because of the use of a different EOS) with the same mass,  $\kappa_2^T$  would be approximately given by  $\kappa_2^T \sim 73(R_A/11.466 \text{ km})^5$

One sees in Table I that the dimensionless tidal parameter  $\kappa_2^T$  is a strongly decreasing function of the mass ratio. This is analytically understood by looking at Eq. (25). If the label  $B$  refers to a black hole (so that  $k_\ell^B = 0$ ), denoting  $q \equiv M_{BH}/M_{NS} = M_B/M_A$ , we have  $\kappa_\ell^T = (\kappa_\ell^T)^A$  where

$$(\kappa_\ell^T)^A = 2 \frac{k_\ell^A}{c_A^{2\ell+1}} \frac{q}{(1+q)^{2\ell+1}}. \quad (26)$$

Here  $c_A$  denotes as above the compactness of the NS. Therefore, as soon as the mass ratio  $q$  is significantly larger than one, we see that  $(\kappa_\ell^T)^A$  contains a small factor  $q^{-2\ell}$  that suppresses the tidal contribution. As a consequence, GW-observable tidal effects will be strongly suppressed in realistic BHNS systems. Note, however, that it might be quite useful to compare numerical relativity simulations of “artificial” BHNS systems of mass ratio  $q \sim 1$  to their EOB description to probe the analytical understanding of the late inspiral and plunge phase.

In particular, we note that, as a function of  $q$ ,  $\kappa_2^T \propto q/(1+q)^5$  vanishes both when  $q \rightarrow 0$  and  $q \rightarrow \infty$  and reaches a maximum value when  $q = M_{BH}/M_{NS} = 1/4$ . Moreover the maximum value of  $\kappa_2^T$  is larger than the value of  $\kappa_2^T$  for a corresponding *equal-mass* BNS system by a factor  $4^6/5^5 = 1.311$ . We suggest that the numerical study of such astrophysically irrelevant BHNS systems (with  $M_{BH}/M_{NS} \sim 1/4$ ) can be quite useful for improving our understanding of tidal interactions in strongly-interacting (near contact) regimes.

### C. Parametrizing higher-order dynamical tidal corrections

Above we discussed the *leading order* (LO) contribution of tidal interactions to the EOB “radial potential”  $A(r)$ . We also discussed the structure of sub-leading (post-Newtonian) contributions to tidal interactions, Eq. (17). Comparing the structure (17) to the part of the EOB action linear in  $A^{\text{tidal}}$ , which is proportional to the product of  $A^{\text{tidal}}$  by reduced mass  $\mu = M^A M^B / (M^A + M^B)$ , we see that the general structure of the tidal contributions to the  $A(r)$  potential is

$$A_{\mu_A}^{\text{tidal}} \sim \frac{M^A + M^B}{M^A M^B} \mu^A \frac{(GM^B)^2}{r^{\ell+2}} \times \left[ 1 + \frac{GM^A}{r} + \frac{GM^B}{r} + \left( \frac{GM^A}{r} + \frac{GM^B}{r} \right)^2 + \dots \right] \quad (27)$$

where we invoked dimensional analysis to insert appropriate powers of the (EOB) radial separation  $r$ . [Contrary to the action (17) which also depends on velocities (and higher-derivatives), the EOB radial potential depends only on the radius  $r$ .]

In other words, if we separate, for each multipolar order, the  $\mu_A$  and  $\mu_B$  contributions to  $A^{\text{tidal}}$ ,

$$A^{\text{tidal}} = \sum_{\ell \geq 2} A^{\mu_A^A} + \sum_{\ell \geq 2} A^{\mu_B^B}, \quad (28)$$

we can write

$$A^{\mu_A^A} = A_{\text{LO}}^{\mu_A^A} \left[ 1 + \alpha_1^{A(\ell)} u + \alpha_2^{A(\ell)} u^2 + \alpha_3^{A(\ell)} u^3 \dots \right], \quad (29)$$

where

$$A_{\text{LO}}^{\mu_A^A} \equiv -\kappa_\ell^A u^{2\ell+2} \quad (30)$$

is the part of  $A_{\text{LO}}^{\text{tidal}}$ , Eq. (23), which is linear in  $\mu_\ell^A$ , or  $k_\ell^A$ , i.e.

$$\kappa_\ell^A = 2 k_\ell^A \frac{M_B}{M_A} \left( \frac{R_A c_0^2}{G(M_A + M_B)} \right)^{2\ell+1}. \quad (31)$$

Similarly, one will have

$$A^{\mu_B^B} = A_{\text{LO}}^{\mu_B^B} \left[ 1 + \alpha_1^{B(\ell)} u + \alpha_2^{B(\ell)} u^2 + \alpha_3^{B(\ell)} u^3 + \dots \right] \quad (32)$$

The coefficient  $\alpha_1^{A(\ell)}$  represents the next to leading order (NLO) fractional correction to the leading order  $A_{\text{LO}}^{\mu_A}$  (i.e. a 1PN fractional correction), while  $\alpha_2^{A(\ell)}$  represents the next-to-next to leading order (NNLO) correction (i.e. a 2PN fractional correction), etc. These coefficients are not pure numbers, but rather function of the two dimensionless mass ratios

$$X_A \equiv \frac{M_A}{M_A + M_B}, \quad (33)$$

$$X_B \equiv \frac{M_B}{M_A + M_B} \equiv 1 - X_A. \quad (34)$$

The coefficients entering Eq. (32) are obtained from those entering (29) by the interchange of  $X_A$  and  $X_B$ , i.e.  $\alpha_n^{A(\ell)}(X_A, X_B) \equiv \alpha_n^{B(\ell)}(X_B, X_A)$ . The symbolic structure (27) would naively suggest that  $\alpha_1^{A(\ell)}$  is a linear combination of  $X_A$  and  $X_B$  and that  $\alpha_2^{A(\ell)}$  is a combination of  $X_A^2$ ,  $X_A X_B$  and  $X_B^2$ . However, as the reformulation of (17) in terms of an EOB potential (27) involves a ‘‘contact transformation’’ that depends on the symmetric mass ratio  $\nu \equiv X_A X_B$  (see Ref. [32]), the mass-ratio dependence of  $\alpha_n^{A(\ell)}$  might be more complicated. Note that, by using the identity  $X_A + X_B \equiv 1$ , one can, e.g., express  $\alpha_n^{A(\ell)}$  in terms of  $X_A$  only. [Then  $\alpha_n^{B(\ell)}$  will be the same function of  $X_B$  than  $\alpha_n^{A(\ell)}$  of  $X_A$ .] Note also that, if one wishes, one can, for each value of  $\ell$  factorize the total LO terms  $-\kappa_\ell^T u^{2\ell+2}$ , and write

$$A^{\text{tidal}} = \sum_{\ell \geq 2} -\kappa_\ell^T u^{2\ell+2} \hat{A}_\ell^{\text{tidal}}, \quad (35)$$

where

$$\hat{A}_\ell^{\text{tidal}} \equiv 1 + \bar{\alpha}_1^{(\ell)} u + \bar{\alpha}_2^{(\ell)} u^2 + \dots, \quad (36)$$

with

$$\bar{\alpha}_n^{(\ell)} \equiv \frac{\kappa_\ell^A \alpha_n^{A(\ell)} + \kappa_\ell^B \alpha_n^{B(\ell)}}{\kappa_\ell^A + \kappa_\ell^B}. \quad (37)$$

Using Eqs. (4.27) and (4.29) of [30], or Eq. (3.33) of [31], together with effective action techniques, a recent calculation [29] gave the following result for the 1PN coefficient of multipolar order  $\ell = 2$ ,  $\alpha_1^{A(2)}$ , namely

$$\alpha_1^{A(2)} = \frac{5}{2} X_A. \quad (38)$$

More work is needed to determine the higher degree and/or higher order coefficients  $\alpha_n^{A(\ell)}(X_A, X_B)$ , and thereby the coefficients  $\bar{\alpha}_n^{(\ell)}$  entering Eq. (37). Below, we shall focus on the equal-mass case where the coefficients  $\alpha_n^{A(\ell)}$  become pure numbers.

Here we shall explore three possible proposals for including higher-order PN corrections in tidal effects. The first proposal consists in truncating Eq. (36) at 1PN order in a straightforward ‘‘Taylor’’ way, i.e. to consider a

PN correcting factor to the EOB radial potential of the form

$$\hat{A}_\ell^{\text{tidal}} = 1 + \bar{\alpha}_1^{(\ell)} u. \quad (39)$$

The second proposal consists in considering a PN correcting factor which has a ‘‘Padé-resummed’’ structure, i.e.

$$\hat{A}_\ell^{\text{tidal}} = \left(1 - \bar{\alpha}_1^{(\ell)} u\right)^{-1}. \quad (40)$$

Our third proposal consists in considering a PN correcting factor which would result from having a ‘‘shift’’ between the EOB radial coordinate and the radial coordinate appearing most naturally in a Newtonian-like tidal interaction ( $\propto 1/r^{2\ell+2}$ ).

$$\hat{A}_\ell^{\text{tidal}} = \left(1 - \tilde{\alpha}_1^{(\ell)} u\right)^{-(2\ell+2)}. \quad (41)$$

We use here a different notation for the 1PN coefficient,  $\tilde{\alpha}_1^{(\ell)}$ , as a reminder that, for instance, when  $\ell = 2$ , the parametrization (41) corresponds to a 1PN coefficient in the parametrization (39) given by

$$\bar{\alpha}_1^{(2)} = 6 \tilde{\alpha}_1^{(2)}. \quad (42)$$

#### IV. COMPARING EOB TO NUMERICAL RELATIVITY RESULTS ON ‘‘WAVELESS’’ CIRCULAR BINARIES

The aim of this section is to compare stationary quasi-circular configurations of neutron star binaries computed, on the one hand, in the analytical framework outlined above and, on the other hand, in the numerical framework recently implemented by Uryū et al. [15] (see also [16]). The quantity from both frameworks that we shall compare is the binding energy  $E_b$  as a function of the orbital frequency  $\Omega$ .

##### A. Tidally interacting BNS circular configurations in the EOB framework

###### 1. BNS binding energy in the EOB framework

As an application of the formalism discussed so far, we consider in this section binaries in exactly circular orbits, in absence of radiative effects (these will be discussed in the following section).

As the EOB formalism is based on a Hamiltonian description of the conservative dynamics, the stable circular orbits correspond to minima, with respect to  $r$ , of the radial potential  $H_{\text{EOB}}^{\text{radial}}(r, p_\varphi) \equiv H_{\text{EOB}}(r, p_{r_*} = 0, p_\varphi)$ . Minimizing  $H_{\text{EOB}}^{\text{radial}}(r, p_\varphi)$  is equivalent to minimizing the corresponding effective Hamiltonian  $\hat{H}_{\text{eff}}$ , or, its square,

i.e.

$$\begin{aligned} (\hat{H}_{\text{eff}}^{\text{radial}})^2(r, p_\varphi) &= A(r) \left( 1 + \frac{p_\varphi^2}{r^2} \right) \\ &\equiv A(u) + p_\varphi^2 B(u). \end{aligned} \quad (43)$$

Here, we have used the short-hand notation  $u \equiv 1/r = GM/R$  and  $B(u) \equiv u^2 A(u)$ . Minimizing (43) with respect to  $r$  (or, equivalently,  $u$ ), for a given (scaled) total angular momentum  $p_\varphi \equiv J^{\text{tot}}/GM\mu$ , yields the following equation

$$A'(u) + p_\varphi^2 B'(u) = 0, \quad (44)$$

where the prime denotes a  $u$ -derivative. This leads to the following parametric representation of the squared angular momentum:

$$j^2(u) = -\frac{A'(u)}{(u^2 A(u))'} \quad (\text{circular orbits}), \quad (45)$$

where we use the letter  $j$  to denote the value of  $p_\varphi$  along the sequence of circular orbits. Inserting this  $u$ -parametric representation of  $j^2$  in Eq. (19) defines the  $u$ -parametric representation of the effective Hamiltonian  $\hat{H}_{\text{eff}}(u)$ . We can then obtain (at least numerically)  $\hat{H}_{\text{eff}}$  as a function of  $x$  by eliminating  $u$  between  $\hat{H}_{\text{eff}}(u)$  and the corresponding  $u$ -parametric representation of the frequency parameter  $x = (GM\Omega/c^3)^{2/3}$  obtained by the angular Hamilton equation of motion in the circular case

$$M\Omega(u) = \frac{1}{\mu} \frac{\partial H_{\text{EOB}}}{\partial j} = \frac{MA(u)j(u)u^2}{H_{\text{real}}\hat{H}_{\text{eff}}}, \quad (46)$$

where  $H_{\text{real}}$  denotes the real EOB Hamiltonian

$$H_{\text{EOB}} = M\sqrt{1 + 2\nu(\hat{H}_{\text{eff}} - 1)}. \quad (47)$$

In this situation, the binding energy  $E_b$  of the system is simply given by

$$E_b(\Omega) = H_{\text{EOB}} - M = M \left\{ \sqrt{1 + 2\nu(\hat{H}_{\text{eff}} - 1)} - 1 \right\}, \quad (48)$$

where  $M$  denotes, as above, the total mass  $M = M_A + M_B$  of the system, and where one must eliminate  $u$  between Eq. (46) and Eq. (48) to express the r.h.s. in terms of  $\Omega$ . Note that the function  $E_b(\Omega)$  depends also on the choice of the following parameters:  $\kappa_\ell^T$ ,  $\alpha_1^{A(\ell)}$  and  $\alpha_1^{B(\ell)}$ . Here we shall focus on the equal-mass case, and consider the dependence of  $E_b(\Omega)$  only on  $(\kappa_2^T, \kappa_3^T, \kappa_4^T)$  and restrict the parametrization of 1PN tidal effects to the consideration of a *single* 1PN tidal parameter  $\bar{\alpha}_1$  that is taken to be the same for the three values of  $\ell$  that we consider. In addition, we will incorporate 1PN corrections to tidal effects in the three aforementioned functional forms, Eq. (39)-(41) and contrast their performances.

## 2. BNS binding energy in the PN framework

We also want to contrast the performance of the EOB approach (which represents a resummation of the dynamics of the binary system) with the “standard” non-resummed PN-based description of the binding energy of tidally interacting BNS, as used for instance in Ref. [37]. The PN-expanded binding energy is written in the form

$$E_b(\Omega) = E_{\text{point-mass}}(\Omega) + E^{\text{tidal}}(\Omega), \quad (49)$$

where

$$\begin{aligned} E_{\text{point-mass}}(\Omega) &= -\frac{\mu}{2}x \left\{ 1 - \left( \frac{3}{4} + \frac{1}{12}\nu \right) x \right. \\ &\quad - \left( \frac{27}{8} - \frac{19}{8}\nu + \frac{1}{24}\nu^2 \right) x^2 \\ &\quad \left. - \left( \frac{675}{64} - \left[ \frac{34445}{576} - \frac{205}{96}\pi^2 \right] \nu + \frac{155}{96}\nu^2 + \frac{35}{5184}\nu^3 \right) x^3 \right\}, \end{aligned} \quad (50)$$

is the 3PN accurate post-Newtonian binding energy of two point-masses as function of the orbital frequency parameter  $x = (GM\Omega/c^3)^{2/3}$  [19, 38]. The expression of the tidal contribution  $E^{\text{tidal}}(\Omega)$  can be obtained for all values of the multipolar index  $\ell$  by noting the following. Any (perturbative) power-law radial contribution to the interaction Hamiltonian of the form

$$\delta H(r) = -\frac{c_n}{r^n} \quad (51)$$

is easily shown to contribute a corresponding term

$$\delta E_b(\Omega) = + \left( \frac{2}{3}n - 1 \right) \frac{c_n}{r_\Omega^n}, \quad (52)$$

where it should be noted that the sign of the tidal contribution flips between the Hamiltonian and the binding energy expressed as a function of the orbital frequency ( $r_\Omega$  denoting the Newtonian value of  $r$  corresponding to a given circular orbit of frequency  $\Omega$ ). As a result, we have the leading order contribution to the PN-tidal contribution

$$E_{\text{LO}}^{\text{tidal}}(\Omega) = +\frac{\mu}{2} \sum_{\ell \geq 2} \left[ \frac{2}{3}(2\ell + 2) - 1 \right] \kappa_\ell^T x^{2\ell+2}. \quad (53)$$

We shall also explore the effect of correcting  $E_{\text{LO}}^{\text{tidal}}$  by a fractional 1PN contribution, i.e. to employ a PN tidal contribution of the form

$$E^{\text{tidal}}(x) = (1 + \bar{\alpha}_1 x) E_{\text{LO}}^{\text{tidal}}(x). \quad (54)$$

where the (approximate) link with the previously defined  $\bar{\alpha}_1$  is

$$\bar{\alpha}'_1 = \frac{11}{9}\bar{\alpha}_1. \quad (55)$$

Here the numerical coefficient 11/9 arises as a consequence of the factor  $2n/3 - 1$  in the result above (considered for  $n = 6$  and  $n = 7$ ).

## B. BNS circular configurations in numerical relativity

### 1. Numerical framework of Uryū et al.

In a recent paper, Uryū et al. [15] constructed BNS systems in quasi-circular orbits by solving numerically the full set of Einstein’s equations. The important advance of this work with respect to previous analyses is the fact that Einstein equations are solved for all metric components, including the nonconformally flat part of the spatial metric. This goes beyond the common *conformally flat* approximation that is usually employed for the spatial geometry. The conformally flat approximation introduced systematic errors which enter the PN expansion already at the 2PN level [see the detailed calculation in the Appendix B of Ref. [35]]. Consistently with this analytical argument, it was found in Ref. [15] that the difference between conformally flat and nonconformally flat calculations is so large that it can mask the effect of tidal interaction for close systems. See, in this respect, the location of the conformally flat (IWM) binding energy curves in the two upper panels of Fig. 3 in Ref. [15]. Below we shall however emphasize that the nonconformally flat calculations of [15] still introduce significant systematic errors which enter the PN expansion *at the 3PN level*.

Since the new nonconformally flat results of Uryū et al. represent a definitive improvement with respect to previous calculations, it is appealing to see to what extent these new results agree with existing analytical descriptions. We extracted from Ref. [15] the six models which present the highest computational accuracy. These models were obtained by using EOS labelled 2H, HB, 2B, SLy, FPS and BGN1H1. These labels refer to piecewise polytropic EOS. Note that in the case of SLy, FPS and BGN1H1 the corresponding piecewise polytropic EOS were proposed in Ref. [39] as approximations to original tabulated EOS. In the case of FPS and SLy, this implies that the tidal coefficients  $k_\ell$  that we have computed for this work differ (by  $\sim 20\%$ ) from the ones that we had previously computed in Ref. [13] that used the original tabulated EOS. For example, in the case of a neutron star model described by the SLy EOS and having a compactness  $c = 0.176$  (which corresponds to a mass of  $1.4M_\odot$ ), we obtain a dimensionless Love number  $k_2^{(\text{tab})} = 0.07699$  (which is consistent with the first line of Table I of Ref. [12]) if we use the tabulated EOS, while we obtain  $k_2^{(\text{ppoly})} = 0.09123$  if we use the piece-wise polytropic EOS. Note that the piece-wise polytropic result is 18.5% larger than the tabulated one. This suggests that one should refine the piece-wise polytropic approximation to realistic tabulated EOS by incorporating  $k_2$  within the set of observables that are fitted.

Among the six EOS that we retain, three, i.e. 2H, HB and 2B, use two polytropic intervals, while the other three, i.e. SLy, FPS and BGN1H1, use four polytropic

intervals. We will thus have one dividing density<sup>3</sup>, denoted by  $\rho_0$ , for 2H, HB and 2B, and three dividing densities,  $(\rho_0, \rho_1, \rho_2)$ , for SLy, FPS and BGN1H1. Here,  $\rho_0$  indicates the dividing density between the lower density interval that approximates the subnuclear density part of the EOS (the crust) and the supernuclear density part. The values of (the base-ten logarithm of)  $\rho_0$  are displayed in the first column of Table I. For all EOS, the lower density interval (“crust”) is approximated by setting  $(\Gamma_0, K_0) = (1.35692, 3.59389 \times 10^{13})$ , where  $K_0$  (here is in cgs units) gives the pressure  $p$  in dyn/cm<sup>2</sup>. The other dividing densities (for the four-parameter EOS) are fixed as  $\rho_1 = 10^{14.7}$  and  $\rho_2 = 10^{15}$ . The corresponding adiabatic indices,  $\{\Gamma_1, \Gamma_2, \Gamma_3\}$ , taken from [15, 39] are also given in Table I. For the implementation of the piecewise polytropic EOS we follow the procedure explained in Sec. III of [39] and in Sec. IID of [15].

For each selected EOS, we computed the sequence of equilibrium models with the related Love numbers  $k_\ell$  up to  $\ell = 4$ . For the compactness corresponding to those used in [15] we display in Table II the  $k_\ell$ ’s together with the values of mass and radius that we obtained from our calculation, to check consistency with the corresponding values of Table III of [15]. The small differences (at the  $10^{-3}$ ) level are probably due to the fact that we use the finite-digit value of the dividing density  $\rho_0$  that they published.

### 2. Subtracting tidal effects from NR data

Let us start by noting two facts, that can be checked from the analytical expressions above, about the dependence of the binding energy on the tidal parameters  $\kappa_\ell^T$ : i) this dependence is to a very good approximation *linear* and ii) the numerical effect of the  $\kappa_2^T$  strongly dominates over that of the higher degree  $\kappa_\ell^T$ ’s. For example, if we take the tidal coefficients listed in Table I (which correspond to the SLy EOS, which yields a radius  $\sim 11.5$  km for  $1.35M_\odot$ , which is in the middle of the realistic range of NS radii) we find that the tidal contributions to the binding energy would reach, if they were extended to the maximum frequency that we shall explore here, namely  $M\Omega_{\text{max}} = 0.060$ , the following values: the  $\kappa_2^T$  contribution to  $E_b/M$  is  $\sim 3.6 \times 10^{-4}$ ; the  $\kappa_3^T$  contribution is smaller than the  $\kappa_2^T$  by a factor 0.053, and the  $\kappa_4^T$  is smaller than the  $\kappa_2^T$  one by a factor  $\sim 3.85 \times 10^{-3}$ .

These two facts allow us to *approximately subtract tidal effects from NR data*. Indeed, if we assume that the binding energy computed with a certain equation state  $(EOS)_I$  is approximately given by

$$E_b(\Omega; I) \approx h_0(\Omega) + (\kappa_2^T)_I h_2(\Omega) \quad (56)$$

<sup>3</sup> Here, following the notation of [39], we use the letter  $\rho$  to denote the rest-mass (baryon) density which was denoted by  $\mu$  in our previous work [13]

TABLE II: Properties of NS models considered discussed in the numerical analysis of Ref. [15]. The EOS are represented as piece-wise-polytropic functions (on four intervals) as proposed in [39, 40]. For the models considered, the present table is compatible with Table III of [15]. From left to right, the columns report: the dividing density between the low-density part (the crust) and the higher density part of the EOS; the four adiabatic indices for each polytropic interval,  $\{\Gamma_0, \Gamma_1, \Gamma_2, \Gamma_3\}$ ; the compactness  $c = M/R$ ; the NS mass  $M$  and the NS radius  $R$ ; the Love numbers  $k_2$ ,  $k_3$  and  $k_4$ .

Model	$\log(\rho_0)$	$\Gamma_0$	$\Gamma_1$	$\Gamma_2$	$\Gamma_3$	$M/R$	$M$	$R$	$k_2$	$k_3$	$k_4$
2H	13.847	1.35692	3	3	3	0.13097	1.3507	15.229	0.1342	0.0407	0.0168
HB	14.151	1.35692	3	3	3	0.17181	1.3507	11.608	0.0946	0.0260	0.0097
2B	14.334	1.35692	3	3	3	0.20500	1.3505	9.728	0.0686	0.0174	0.0059
SLy	14.165	1.35692	3.005	2.988	2.851	0.17385	1.3499	11.466	0.0928	0.0254	0.0095
FPS	14.220	1.35692	2.985	2.863	2.600	0.18631	1.3511	10.709	0.0805	0.0214	0.0077
BGN1H1	14.110	1.35692	3.258	1.472	2.464	0.15792	1.3490	12.614	0.1059	0.0307	0.0120

we can use the NR data for two different EOS, labelled by  $(I, J)$  to compute, *separately*

$$h_0(\Omega) \approx \frac{(\kappa_2^T)_I E_b(J) - (\kappa_2^T)_J E_b(I)}{(\kappa_2^T)_I - (\kappa_2^T)_J}, \quad (57)$$

$$h_2(\Omega) \approx \frac{E_b(I) - E_b(J)}{(\kappa_2^T)_I - (\kappa_2^T)_J}. \quad (58)$$

Most importantly we see that Eq. (57) allows us to compute from the binding energies of two BNS sequences a third binding energy function,  $h_0$ , which approximately represents the binding energy of *non tidally interacting* neutron stars, i.e. the binding energy curve of two point-masses. The result of computing the r.h.s. of Eq. (57) for five pairs  $(I, J)$  of EOS having sufficiently different  $\kappa_2^T$ 's is displayed in the left panel of Fig. 1. Two important lessons can be drawn from this figure: i) The subtraction procedure defined by Eq. (57) is remarkably able to define “tidal-free” energy curves that are essentially on top of each other; this confirms that our procedure succeeds in subtracting out the EOS-dependence of the binding energy curves; ii) However, the resulting “universal”  $h_0$  curve still differs significantly both from the EOB point-mass curve (black solid line) and the PN point-mass one (black dashed line). This second issue will be addressed in the next subsection.

We shall not display here the result of computing the  $h_2$  part of the binding energy curve, Eq. (58), because it is more sensitive than  $h_0$  both to numerical noise (in the original NR data) and to the presence of higher-order tidal PN contributions. Below, we shall address the issue of determining the tidal contributions to  $E_b$  with a different approach.

### 3. Detecting and subtracting systematic errors in NR data

Here we address the issue ii) mentioned in the previous subsection. Indeed, our subtraction procedure has given us access to the “universal”, EOS-independent part of

the energy curve  $h_0$ . However, we have seen that  $h_0$  still significantly differs from the analytical point-mass models. We think that the origin of this discrepancy is the presence of remaining “systematic errors” in the current nonconformally flat approach to BNS systems. Though the nonconformally flat integration scheme of Uryū et al. is an improvement over previous work, it is however still only an approximation to the exact solution describing two BNS interacting in a (conservative) “time-symmetric” manner (half-retarded-half-advanced). Here we shall only use the data obtained by Ref. [15] called the “waveless” approximation. In their approach, “waveless” means setting to zero the time-derivative of the conformal spatial metric (in a certain gauge):  $\partial_t \tilde{\gamma}_{ab} = 0$ . As the NR gauge is rather similar to the ADM-TT gauge used in the 3PN calculation of the interaction Hamiltonian of a two point-mass system in Refs. [19, 41], we can see, by looking at the analytical expression of the 3PN-accurate ADM Hamiltonian, that neglecting the terms containing  $\pi_{ab}^{TT} \sim \partial_t \tilde{\gamma}_{ab}$  means neglecting some of the terms that contribute at the *3PN level*. [The simplest of these terms being the “kinetic energy” term proportional to  $\int d^3x (\pi_{ab}^{TT})^2$ ]. This analytical argument suggests that the current NR data miss some 3PN contributions, i.e. they miss some terms proportional to  $x^4$  in the binding energy curve. We are therefore entitled in assuming that the discrepancy displayed in the left-panel of Fig. 1 between the NR  $h_0$  and the point-mass analytical curves is, to leading order, given by an expression of the type  $\Delta E_b(\Omega) = \delta x^4$  with an EOS-independent numerical coefficient  $\delta$  that we expect to be of order unity. Indeed, the right panel of Fig. (1) exhibits the fact that, by subtracting  $\Delta E_b(\Omega) = \delta x^4$ , with  $\delta = 0.8$  (see below) from all the individual  $h_0$  curves, we can reach a good visual agreement with both analytical point-mass models. [Note that the approximate “best-fit” value of  $\delta$  is mainly determined by the discrepancy NR/AR on the lower frequency part of the panel, say for  $M\Omega < 0.035$  where the contribution to tidal effects is relatively negligible].

The remaining differences in this right panel are com-

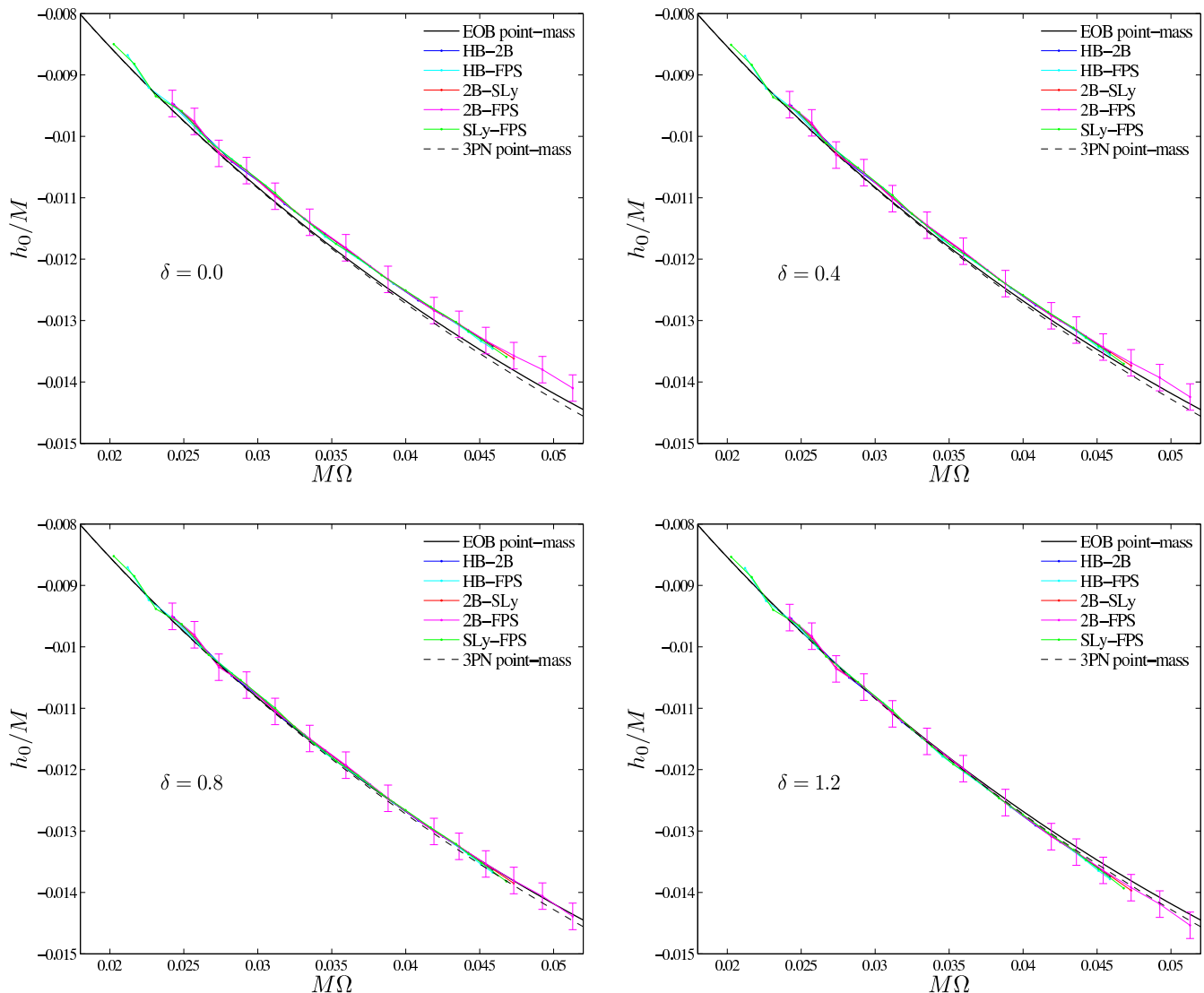


FIG. 1: Comparison between various  $\delta$ -corrected  $h_0$ 's (defined in Eq. (57)) and the EOB (resummed, solid line) and 3PN (nonresummed, dashed line) point-mass representations of the binding energy.

patible with the known level of numerical errors in the NR data (see Fig. 4 of Ref. [15]). Indeed [15] has used the virial theorem to gauge some of the systematic errors in their calculation by comparing two measures of the total mass of the system (Komar and ADM). The resulting (absolute value) differences in binding energy, say  $\delta^v E_b$  are in general at the level  $10^{-4}M$ . We used these differences to estimate formal “error-bars” on the various energy curves that we use in this work. More precisely, in  $E_b$  energy curves we add error bars of one-sided amplitude  $\pm \frac{1}{2}\delta E_b$ , so that the length of the two-sided error bars corresponds to the “virial” error. As Fig. 1 concerns a quantity,  $h_0$ , defined as a linear combination of NR data (see Eq. (57)), we conservatively estimated error bars on the  $h_0$  curve corresponding to the pair 2B-FPS by linearly combining in absolute values the corresponding individual errors. We use this error bar to gauge the qual-

ity of the other  $h_0$  curves (which do not extend as far in the high frequency range). This conservative estimate of the total error seems appropriate to the present situation where the errors are not random, but rather systematic. [Note, however, that these “error-bars” seem to be too conservative in the lower frequency part of the panels because they exceed the “distance” between the  $h_0$  curves and the point-mass models.] Using these error bars we can now roughly estimate a range of acceptable values of the NR correcting parameter  $\delta$ . As illustrated in the four panels of Fig. 1, the range  $0.4 \leq \delta \leq 1.2$  is such that the  $\delta$ -corrected NR-deduced  $h_0$  curves are within “one formal sigma” from both point-mass analytical models. We shall use this range below to estimate a corresponding range of probable values of the 1PN tidal parameter  $\bar{\alpha}_1^{(2)}$ .

4. *Least-square analysis: constraining next-to-leading order (1PN) tidal effects from numerical relativity data*

In this subsection we shall firm up the previous analysis and make it more quantitative by using a  $\chi^2$  procedure. For each EOS, labelled by index  $I$ , we have 20 NR data points, Ref. [15],  $E_b^{\text{Ury}\bar{u}}(x_{n_I}; I)$ , where the index  $n_I$  varies from one to twenty. We retain in our analysis six EOS;  $I=(2\text{H}, \text{HB}, 2\text{B}, \text{FPS}, \text{SLy}, \text{BGN1H1})$ . Let us then define the following formal  $\chi^2$  function, measuring the (squared) “distance” between NR and EOB:

$$\chi^2(\bar{\alpha}_1, \delta) = \sum_{I,n} \left[ \frac{(E_b^{\text{Ury}\bar{u}}(x_n; I) - \delta x_n^4)}{M} - \frac{E_b^{\text{EOB}}(x_n; \bar{\alpha}_1, I)}{M} \right]^2. \quad (59)$$

Here,  $x = \Omega^{2/3}$  and the index  $n$  runs (for each EOS label  $I$ ) over the sample of numerical data from one to twenty, so that  $\chi^2$  contains 120 terms in all. We are interested in studying the dependence of  $\chi^2$  over the two variables  $(\delta, \bar{\alpha}_1)$ . Here  $\delta$  denotes the coefficient of a 3PN subtraction to NR data of the type that we discussed in the previous subsection (as motivated by the neglect of some 3PN terms in the “waveless” approximation). As explained above, we shall restrict the variation of  $\delta$  to the range  $0.4 \leq \delta \leq 1.2$ . For simplicity, we shall actually sample this interval through the three values  $\delta = (0.4, 0.8, 1.2)$ . On the other hand, the coefficient  $\bar{\alpha}_1$  parametrizes possible next-to-leading order (NLO) 1PN correction to the tidal effects. We will use the three different descriptions of NLO tidal effects delineated in Eqs. (39)-(41) above.

We wish to use the least-square method, i.e., minimizing the EOB-NR “distance” function  $\chi^2(\bar{\alpha}_1, \delta)$ , to constrain the values of  $(\bar{\alpha}_1, \delta)$ . However, we find that  $\chi^2(\bar{\alpha}_1, \delta)$  remains close (on the scale of the NR error bars) to its global minimum in a “valley” which extends over a significant region of an  $(\bar{\alpha}_1, \delta)$  plane. This means that, given the present error level in numerical data, we cannot meaningfully and simultaneously select preferred values for  $(\bar{\alpha}_1, \delta)$ . As a substitute, we shall exhibit the sections of the  $\chi^2$  valley that correspond to the three values of  $\delta$  selected visually above in Fig. 1. In other words, we now fix  $\delta$  (to one of its three values) in Eq. (59) and consider the dependence of  $\chi^2$  on  $\bar{\alpha}_1$ . The resulting one-dimensional plots are exhibited in Fig. 2.

Each panel of Fig. 2 corresponds to a different modelization of NLO tidal effects: “Taylor” (upper panel, Eq. (39)), “Padé” (middle panel), Eq. (40) and “radial-shift” (lower panel), Eq. (41). In addition, each panel contains three curves corresponding to the three above-selected values of  $\delta$ :  $\delta = 0.4$  (dash-dot line, right-most curve),  $\delta = 0.8$  (solid-line, middle curve), and  $\delta = 1.2$  (dashed-line, left-most curve).

Let us start by focussing on the (solid) curves corresponding to the “central” value of  $\delta$ ,  $\delta = 0.8$ . We see that the preferred values of  $\bar{\alpha}_1$  that they select (minimum of the curves) are  $\bar{\alpha}_1 \approx 7$  for the Taylor model,  $\bar{\alpha}_1 \approx 3.5$  for the Padé model and  $\bar{\alpha}_1 \approx 4.5$  for the “radial-shift” model. This shows that higher order PN

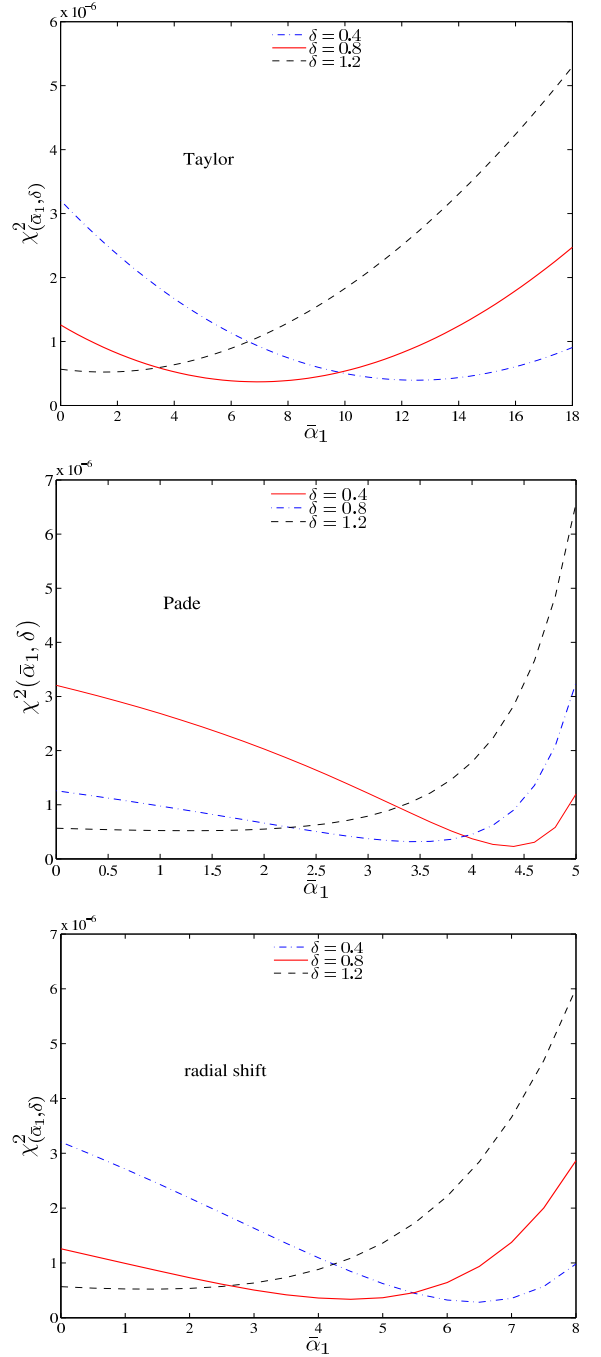


FIG. 2: Sections of the function  $\chi^2(\bar{\alpha}_1, \delta)$  for three values of  $\delta$ . The figure displays the corresponding ranges of allowed values of  $\bar{\alpha}_1$ . Note that, for all models, the minima are rather shallow.

terms (differently included in the different models) have a significant effect on the determination of  $\bar{\alpha}_1$ . Note also that when  $\delta = 1.2$  all the models tend to favour a lower value:  $\bar{\alpha}_1 \sim 1$ . The value of  $\chi^2$  at  $\bar{\alpha}_1 = 0$  and  $\delta = 1.2$  is  $\chi^2(0, 1.2) = 5.665 \times 10^{-7}$ . This formally corresponds to an average (squared) “error level” on the individual NR-EOB energy differences summed in  $\chi^2$  equal

to  $\sqrt{\chi^2(0, 1.2)/120} = 0.687 \times 10^{-4}$ . This level is comparable to the “virial error” on each individual NR data point  $\delta^v E_b/M \sim 10^{-4}$ . It is therefore reasonable to use this level to select a range of values of  $\bar{\alpha}_1$ . Combining this range with the range of values of  $\delta$ 's means that, at this stage, the range of values of  $\bar{\alpha}_1$  that is compatible with the NR data is obtained by taking the level surface  $\chi^2(\bar{\alpha}_1, \delta) = \chi^2(0, 1.2)$  as the admissible bottom of the “valley” in the  $(\bar{\alpha}_1, \delta)$  plane. This leads to the following admissible ranges:  $0 \lesssim \bar{\alpha}_1 \lesssim 15.7$  for the Taylor model;  $0 \lesssim \bar{\alpha}_1 \lesssim 4.8$  for the Padé model;  $0 \lesssim \bar{\alpha}_1 \lesssim 7.5$  for the “radial shift” model. It is clear that at this stage the fact that (as we have argued above) the NR data are “polluted” by some systematic errors (notably linked to unaccounted 3PN effects) prevents us from giving very significant constraints on the value of  $\bar{\alpha}_1$ . Note in particular that the value  $\bar{\alpha}_1 = 5/4 = 1.25$  which follows (in the equal-mass case) from Eq. (38) is compatible with the present NR data (if we allow  $\delta = 1.2$ ). In this respect, it is interesting to note that if we consider a model of the form

$$\hat{A}^{\text{tidal}} = 1 + \bar{\alpha}_1 u + \bar{\alpha}_2 u^2, \quad (60)$$

with  $\bar{\alpha}_1 = 1.25$  and compute the corresponding  $\chi^2$  for the central value  $\delta = 0.8$ , we find that  $\chi^2(\bar{\alpha}_2, 0.8)$  reaches a minimum around  $\bar{\alpha}_2 \approx 40$ . In addition the value of the minimum of the  $\chi^2$  is  $3.20 \times 10^{-7}$  which is slightly better than the performance of the 1PN Taylor model in the upper panel of Fig. 2. This shows again that higher PN tidal effects can play an important role and that the minima exhibited (for the central value  $\delta = 0.8$ ) in the three panels of Fig. 2 should be viewed as “effective” values of  $\bar{\alpha}_1$ . We note in this respect that a situation where higher-PN corrections dominate over the 1PN one is not at all exceptional. For instance, the 1PN contribution to the EOB radial potential  $A(r)$  *vanishes*, its 2PN contribution has a rather small coefficient,  $2\nu$ , while the numerical coefficient of the 3PN contribution  $\nu a_4$  is quite large and significantly modifies the conclusions that one might draw from the first two PN contributions.

Figs. 3 and 4 illustrate the complementary effects of  $\bar{\alpha}_1$  and  $\delta$  at the level of the binding energy  $E_b$ .

Fig. 3 focuses on the 2B EOS model and contrasts (resummed) EOB (top panel) and (nonresummed) PN analytical representations of the binding energy. In both cases, the NR binding energy is corrected by the same amount, that is we assume that  $\delta$  takes its central value  $\delta = 0.8$ . We see on this figure that the effect of the  $\delta$ -correction is comparable to that of the added 1PN tidal contribution. Note that the value of the  $\bar{\alpha}'_1$  parameter needed in the PN expanded case (bottom panel) is significantly larger than the ones needed in the EOB case (for all ways of modeling 1PN tidal contributions).

Fig. 4 illustrates the excellent agreement between the EOB predictions (here considered for  $\bar{\alpha}_1 = 1.25$ ) and the ( $\delta$ -corrected, with  $\delta = 1.2$ ) numerical data for all EOS. The fact that the  $\chi^2$  minima exhibited in Fig. 2 are at a comparable level (for all  $\delta$ 's in the range we considered)

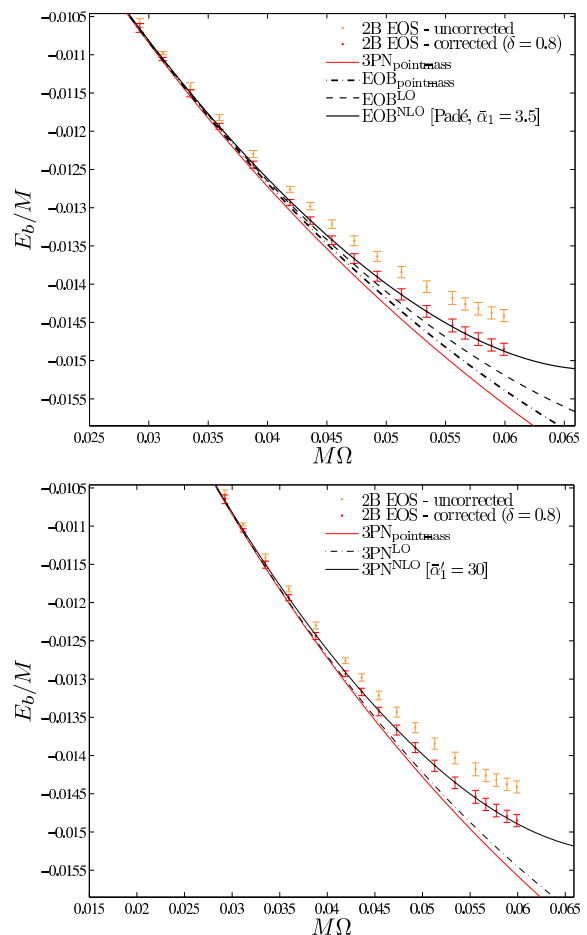


FIG. 3: 2B EOS: Explicit comparison between various analytical representations of the binary binding energy and (corrected) numerical relativity data. The correction parameter is chosen to be  $\delta = 0.8$ . The upper panel refers to EOB (resummed) models. The lower panel to PN (nonresummed) models. For  $\text{EOB}^{\text{NLO}}$  effects, we use their Padé representation, Eq. (40) with  $\bar{\alpha}_1 = 3.5$ . For the  $3\text{PN}^{\text{NLO}}$  model, we use  $\bar{\alpha}'_1 = 30$ .

indicates that a similarly excellent NR/EOB agreement would have been obtained all along an extended valley in the  $(\bar{\alpha}_1, \delta)$  plane. In view of Fig. 3 the same would hold for the NR/PN agreement, at the cost, however, of using, on average, significantly larger values of  $\bar{\alpha}_1$ .

Summarizing: the recent numerical data of Uryū et al. do exhibit the influence of tidal interactions in close BNS systems. However, the presence of systematic errors in the data (due to an imperfect satisfaction -of the helical-Killing-vector condition) partially masks the tidal interactions and does not allow for a clean determination of the coefficients parametrizing tidal effects (and notably their 1PN contributions).

We recommend that new non-conformally flat simulations be performed for several values of the radius  $r_0$  at which the helical-Killing-vector condition is cut off. By studying the dependence of the results on  $r_0$ , it might

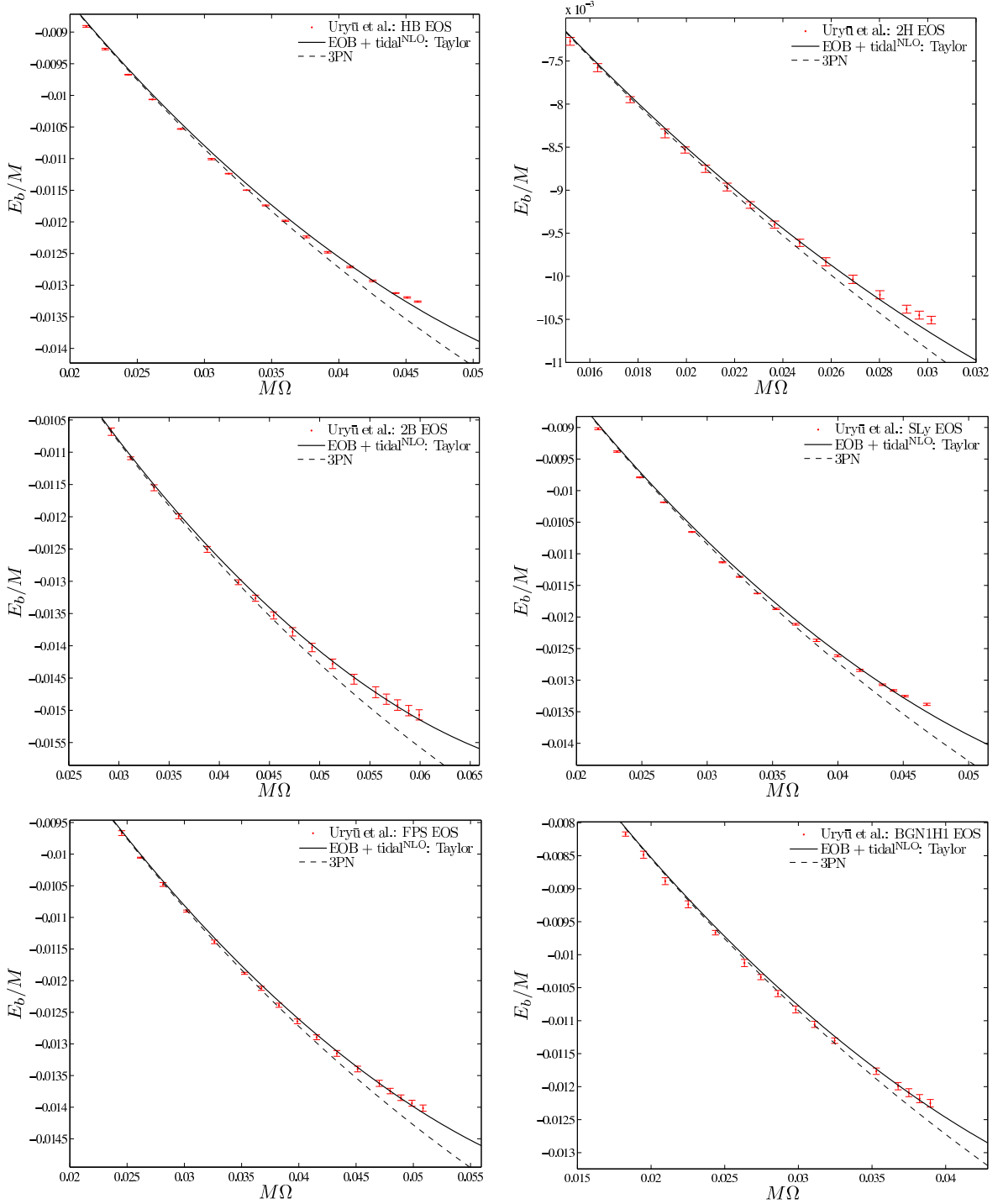


FIG. 4: Global comparison between  $\text{EOB}^{\text{NLO}}$  and NR binding energies. We use the values  $(\bar{\alpha}_1, \delta) = (1.25, 1.2)$ . The 3PN point-mass curve is added to guide the eye.

be possible to extrapolate the results to infinite value of  $r_0$  (as used in analytical calculations), and thereby eliminate the 3PN-level systematic error  $\delta x^4$ .

## V. INCORPORATING RADIATIVE TIDAL EFFECTS IN THE EOB FORMALISM

Besides the specific Hamiltonian (18), (19), the other key ingredients of the EOB formalism are: (i) a specific, “factorized” representation of the multipolar waveforms

$h_{\ell m}$ , and (ii) a resummed estimate of the radiation reaction force  $\mathcal{F}$ , which must be added to the conservative Hamiltonian dynamics (18), (19). In the most recent, and seemingly most accurate, version of the EOB formalism the radiation reaction is analytically computed in terms of the multipolar waveforms. Therefore, it will be enough to estimate here the ‘‘tidal correction’’ to the multipolar waveforms  $h_{\ell m}$ . Following the ‘‘factorization’’ philosophy of Refs. [13, 42] we shall look for tidal-correction factors  $f_{\ell m}^{\text{tidal}} = 1 + \mathcal{O}(\mu, \sigma)$ , such that the EOB waveform would read

$$h_{\ell m} = f_{\ell m}^{\text{tidal}} h_{\ell m}^0. \quad (61)$$

Here  $h_{\ell m}^0$  is the factorized BBH EOB waveform, introduced in [42], and augmented by two next-to-quasi-circular parameters  $(a_1, a_2)$  in Ref. [1]. [Note, however, that, in view of the smallness of the tidal effects on the waveform,  $f_{\ell m}^{\text{tidal}} - 1 \ll 1$ , it would be equivalent to use (as done for the  $A(r)$  potential) an *additive* ansatz:  $h_{\ell m} = h_{\ell m}^0 + h_{\ell m}^{\text{tidal}}$ .]

In principle, one can use the effective action (4), (5) to compute the tidal contributions to the waveform with any required relativistic accuracy (post-Minkowskian and/or post-Newtonian).

Here, we shall focus on the leading PN-order tidal correction to the leading PN waveform, i.e. the  $\ell = 2, m = 2$  partial wave  $h_{22}$ . This will provide the leading tidal correction to the radiation reaction (which is predominantly given by a contribution  $\propto |2\Omega h_{22}|^2$ ).

In that case, a shortcut for computing the tidal correction  $f_{22}^{\text{tidal}}$  consists in noting that the quadrupolar gravito-electric contribution in the action (4) corresponds to adding to the energy-momentum tensor of point-masses an extra contribution  $\Delta T_{(x)}^{\mu\nu} \equiv 2g^{-1/2} \delta\Delta_{\text{nonminimal}} S/\delta g_{\mu\nu}$ , which describes the tidally induced quadrupole moment in each body  $A$ . At the leading ‘‘Newtonian’’ order this means that the quadrupole mass moment  $M_{ij}$  of the system will be

$$M_{ij} = \sum_A \text{STF}_{ij} [M^A z_A^i z_A^j + \mu_2^A G_{ij}^A], \quad (62)$$

where STF denotes a symmetric trace-free projection, and where the second term is the tidally induced quadrupole moment. Replacing the Newtonian value (8) of  $G_{ij}^A$  (computed using Eq. (9)) yields

$$\begin{aligned} M_{ij} &= \sum_A \text{STF}_{ij} \left[ M_A z_A^i z_A^j + 3\mu_2^A G M_B \frac{z_{AB}^i z_{AB}^j}{r_{AB}^5} \right] \\ &= \left( \mu + \sum_A 3\mu_2^A \frac{G M_B}{r_{AB}^5} \right) r_{AB}^2 \hat{n}_{AB}^{ij}, \end{aligned} \quad (63)$$

where  $\mu \equiv M_A M_B / (M_A + M_B)$  is the reduced mass of the binary system, and where we reduced the first expression to the center-of-mass frame. Eq. (63) agrees with Eq. (7) of [10] (in the limit where one neglects the

excitation of the internal radial modes:  $x_n \rightarrow 0$ ). In addition to the explicit tidal modification  $\propto \mu_2^A$  that appears in the first factor of Eq. (63), there is an implicit tidal effect coming from the fact that the EOB waveform is conventionally expressed in terms of the (instantaneous) orbital frequency  $\Omega$  of the binary system. We must then eliminate the relative distance  $r_{AB}$  in Eq. (63) in favor of  $\Omega$ . This is done by using the adiabatic (quasi-circular) Kepler law. The latter is modified by tidal forces:

$$\begin{aligned} \Omega^2 z_{AB}^i &= -\frac{d^2 z_{AB}^i}{dt^2} = -\frac{1}{\mu} \frac{\partial L}{\partial z_{AB}^i} \\ &= \frac{GM}{r_{AB}^3} z_{AB}^i - \frac{1}{\mu} \frac{\partial L^{\text{tidal}}}{\partial z_{AB}^i}. \end{aligned} \quad (64)$$

Differentiating the leading ( $\ell = 2$ ) tidal Lagrangian (16), and keeping only the leading ( $\ell = 2$ ) term yields a modified Kepler law of the form

$$\Omega^2 r_{AB}^3 = GM \left[ 1 + 9 \frac{M_B}{M_A} \frac{G\mu_2^A}{r_{AB}^5} + 9 \frac{M_A}{M_B} \frac{G\mu_2^B}{r_{AB}^5} \right]. \quad (65)$$

Using (65) to solve  $r_{AB}$  in terms of  $\Omega$ , and replacing the (tidally-corrected) answer in (63) finally leads to a quadrupole moment of the form

$$M_{ij} = f_{22}^{\text{tidal}} \mu r_{AB}^2 \hat{n}_{AB}^{ij} \quad (66)$$

with a tidal-correction factor

$$\begin{aligned} f_{22}^{\text{tidal}} &= 1 + \sum_A 3 \frac{G\mu_2^A}{r_{AB}^5} \left( \frac{M_B}{\mu} + 2 \frac{M_B}{M_A} \right) \\ &= 1 + \sum_A 3 \frac{G\mu_2^A}{r_{AB}^5} \left( 1 + 3 \frac{M_B}{M_A} \right) \\ &= 1 + \sum_A 2k_2^A \left( \frac{R_A}{r_{AB}} \right)^5 \left( 1 + 3 \frac{M_B}{M_A} \right). \end{aligned} \quad (67)$$

The factor  $f_{22}^{\text{tidal}}$  is the  $\ell = 2, m = 2$  tidal-correction factor which was introduced in Eq. (61). It remains, however, to eliminate  $r_{AB}$  in terms of  $\Omega$ , or, as used in the waveform of Ref. [42], in terms of the EOB variable  $v_\Omega \equiv r_\Omega \Omega$  introduced in [43]: at the leading order it is enough to use  $GM/c_0^2 r_{AB} = v_\Omega^2 (1 + \mathcal{O}(1/c_0^2))$ . This yields

$$\begin{aligned} f_{22}^{\text{tidal}} &= 1 \\ &+ \left( \sum_A 2k_2^A \left( \frac{R_A c_0^2}{G(M_A + M_B)} \right)^5 \left( 1 + 3 \frac{M_B}{M_A} \right) \right) v_\Omega^{10}. \end{aligned} \quad (68)$$

The result (68) agrees (after squaring it) with Eq. (8c) of Ref. [10] (in the limit  $x_n \rightarrow 0$ ).

Summarizing: we propose to incorporate radiative tidal effects in the EOB formalism by inserting in the

dominant  $\ell = 2$ ,  $m = 2$  waveform, a factor of the form

$$f_{22}^{\text{tidal}} = 1 + \left( \sum_A 2k_2^A \left( \frac{R_A c_0^2}{G(M_A + M_B)} \right)^5 \left( 1 + 3 \frac{M_B}{M_A} \right) \right) v_\Omega^{10} \times (1 + \beta_1 v_\Omega^2), \quad (69)$$

where we included a possible 1PN correction to radiative tidal effects. One then computes a tidal-corrected radiation reaction by using this corrected waveform in the definition of  $\mathcal{F}$  given in [42] and [13]. In principle the (mass-ratio dependent) coefficient  $\beta_1$  can be computed analytically. It can also be “calibrated” by comparing NR data of inspiralling BNS systems to the EOB predictions.

## VI. EOB PREDICTIONS FOR THE MOTION AND RADIATION OF INSPIRALLING COMPACT BINARIES

Having defined a specific EOB way of incorporating tidal effects in the motion and radiation of inspiralling compact binaries (BNS or BHNS) let us study the predictions made by the resulting tidally-extended EOB formalism.

### A. Adiabatic inspiral, “last stable orbit”, and “contact”

Let us start by considering the *adiabatic* approximation to the inspiral, i.e. the approximation in which the inspiral is described as a sequence of circular orbits. In this approximation, a key concept is that of the Last Stable (circular) Orbit (LSO). We saw above the equation determining, in the EOB formalism, the sequence of circular orbits, Eq. (44). For large values of  $p_\varphi$ , and large values of  $r$  (i.e. small values of  $u = 1/r$ ), Eq. (44) has a unique solution  $r = 1/u \simeq p_\varphi^2$ , corresponding to Newtonian circular orbits. However, when  $p_\varphi^2$  decreases (as it does along the sequence of inspiralling orbits driven by radiation reaction), the sequence of stable circular orbits will terminate at certain values  $r_{\text{LSO}} \equiv 1/u_{\text{LSO}}$ ,  $p_{\varphi_{\text{LSO}}}^2$  where there exists a double root of Eq. (44), i.e. a common root of Eq. (44) and

$$A''(u) + p_\varphi^2 B''(u) = 0. \quad (70)$$

The condition determining the radial location of the Last Stable Orbit (LSO) is the vanishing of the determinant

$$\begin{vmatrix} A' & B' \\ A'' & B'' \end{vmatrix}_{\text{LSO}} = A'(u_{\text{LSO}}) B''(u_{\text{LSO}}) - A''(u_{\text{LSO}}) B'(u_{\text{LSO}}) = 0. \quad (71)$$

For instance, in the test-mass limit, and in absence of tidal corrections, i.e. for  $A(u) = 1 - 2u$ ,  $B(u) =$

$u^2 A(u) = u^2 - 2u^3$ , Eq. (71) reads  $-4(1 - 6u_{\text{LSO}}) = 0$ , so that we recover the classic result  $r_{\text{LSO}} = 1/u_{\text{LSO}} = 6$  (i.e.  $r_{\text{LSO}}^{\text{phys}} = 6GM$ ) for the LSO around a Schwarzschild black hole. On the other hand, when inserting in Eq. (71) the complete value of the  $A$  function, i.e. the sum (22), where  $A^0(r; \nu)$  is given by Eq. (21), and  $A^{\text{tidal}}(r)$  by Eq. (23), we see that the LSO predicted by the EOB formalism will depend both on the symmetric mass ratio  $\nu$ , and on the EOB tidal constants  $\kappa_\ell^T$ , Eq. (25). More precisely, these two types of effects (the  $\nu$ -dependent ones which exist already in BBH systems, and the tidal-dependent ones which exist only in BHNS and BNS systems) act in opposite directions. Indeed, the  $\nu$ -dependent contributions tend to make the radial potential  $A(r)$  less attractive (see Eq. (20)), while the tidal ones make  $A(r)$  more attractive. As a consequence,  $\nu$ -effects tend to move the radial location of the LSO towards smaller values ( $r_{\text{LSO}}(\nu) < 6GM$ ), while tidal effects tend to move  $r_{\text{LSO}}$  towards larger values. To avoid gauge effects, it is convenient to measure the location of the (adiabatic) LSO in terms of the corresponding (real) orbital frequency

$$\Omega = \frac{\partial H_{\text{EOB}}}{\partial p_\varphi^{\text{phys}}} = \frac{1}{GM\mu} \frac{\partial H_{\text{EOB}}}{\partial p_\varphi}. \quad (72)$$

Finally, we conclude that the dimensionless orbital frequency  $GM\Omega$  at the LSO is a function of the dimensionless parameters  $\nu$ ,  $\kappa_\ell^T$  which tends to *increase* as  $\nu$  increases, and to *decrease* as  $\kappa_\ell^T$  increases. We have seen above that the tidal coefficients  $\kappa_\ell^T$  generically take rather large numerical values, of order  $\kappa_2^T = \mathcal{O}(100)$ , when  $\ell = 2$ , see Table I. However, they enter the  $A$  function at a higher order in  $u$  than the  $\nu$ -dependent effects. As a consequence, the combination of the influences of  $\nu$  and  $\kappa_2^T, \kappa_3^T, \dots$  leads to orbital LSO frequencies which are sometimes larger, and sometimes smaller than the “Schwarzschild value”  $GM\Omega_{\text{Schw}} = 6^{-3/2} = 0.06804$ . This is illustrated in Table III which lists the values of *twice* the orbital frequency (corresponding to the adiabatic gravitational wave frequency  $\omega_{\ell m}$  for the dominant mode  $\ell = m = 2$ ) for several compactnesses (0.13, 0.17, 0.17385, 0.5) and for two paradigmatic systems: an equal-mass BNS system and a binary black hole system (labelled by its formal compactness  $c = 0.5$ ). Here we took the piece-wise polytropic SLy EOS. Note that one NS mass is smaller than the “canonical”  $1.35M_\odot$  so to explore a smaller compactness. If needed, one can convert the dimensionless frequency  $2GM\Omega$  in Hz by using  $GM_\odot = 4.925490947\mu\text{s} (= 1.476625038 \text{ km})$  so that the conversion factor between  $\hat{\omega} = GM\omega$  and  $f = \omega/2\pi$  is

$$f = \frac{\hat{\omega}}{2\pi GM} = 32.3125 \hat{\omega} \left( \frac{M_\odot}{M} \right) \text{kHz}. \quad (73)$$

We see that, in a BNS system, the LSO frequency is smaller than the “Schwarzschild value”  $2GM\Omega_{\text{Schw}} = 1/(3\sqrt{6}) = 0.136083$  for compactness smaller than about 0.1704. For such system the radius of the LSO is larger than the canonical Schwarzschild  $6GM$ . Note, by comparing BNS to BBH ones, how tidal effects can significantly

change the LSO frequency by more than a factor two! The results shown in Table III have been computed using the leading order, non-PN-corrected EOB description of tidal effects. The inclusion of next-to-leading order effects, notably with  $\bar{\alpha}_1 \sim 6$ , would double the effect of tidal interactions at the LSO and would therefore significantly affect the numbers listed in the table.

In some BNS systems the concept of LSO and LSO frequency has only a formal meaning because the two NS's enter in contact (slightly) before reaching the LSO. This is illustrated in Table III which lists also the value of (twice) the orbital frequency at the moment of “contact”, i.e. when the EOB radial separation  $R$  becomes equal to the sum of the two (areal) radii  $R_A + R_B$ . [We use  $R_B = 2GM_B$  when the companion is a BH.] Note that it is approximately given by the simple analytical formula

$$2GM\Omega_{\text{contact}} \approx 2 \left( \frac{X_A}{c_A} + \frac{X_B}{c_B} \right)^{-3/2}. \quad (74)$$

This definition of “contact” relies on the use of the EOB radial coordinate. As this coordinate is a smooth deformation of the usual areal coordinate, we think that it is a reasonable definition, and we propose here to use the EOB description up to the moment when either the two objects enter in contact, or (if it happens earlier) when the orbital frequency  $\Omega$  reaches a maximum. Note also that Table III illustrates the possible effect (for  $c = 0.13$ ) of NLO (1PN) tidal contributions. This effect is very significant. The second line of the table indicates that, when using a “Taylor” model with  $\bar{\alpha}_1 = 7.0$  (which was the minimum of  $\chi^2$  for the central value of  $\delta$ ), the arrangement of the LSO and touching radius changes. In absence of 1PN correction the contact was reached *before* LSO, while with  $\bar{\alpha}_1 = 7.0$  the contact is reached *after* the LSO, which means that the system undergoes a short “plunge phase” before entering in contact.

In addition to the discussion of the frequency at the moment of contact (i.e. when  $R = R_A + R_B$ ) let us also consider the dimensionless parameter measuring the tidal deformation of the NS labelled  $A$  by its companion  $B$

$$\epsilon_A = \frac{M_B}{R^3} \frac{R_A^3}{M_A}. \quad (75)$$

At contact, ( $R = R_A + R_B$ ), this parameter can be expressed in terms of the two compactnesses  $c_A = GM_A/R_A$  and  $c_B = GM_B/R_B$  as

$$\epsilon_A^{\text{contact}} = \frac{c_B}{c_A} \frac{R_A^2 R_B}{(R_A + R_B)^3}. \quad (76)$$

For a symmetric, equal-mass BNS system, we see that, upon contact,  $\epsilon_A^{\text{contact}} = \epsilon_B^{\text{contact}} = 1/8$ . It was found in [13], and briefly recalled above, that the fractional deformation of the NS  $A$  is given by the product  $h_2^A \epsilon_A$ , where the “shape” Love number  $h_2^A$  is of order 0.8 for a typical NS compactness. This means that, in a symmetric (or near symmetric) BNS system each NS is only

deformed by about 10% at the moment of contact. This motivates our proposal of using the EOB description up to the moment of contact.

In the case of asymmetric BHNS systems (with  $A$  labelling the NS and  $B$  the BH) we can reach a similar general conclusion by noticing that the dimensionless function  $R_A^2 R_B / (R_A + R_B)^3$  (which depends only on the ratio  $R_A/R_B$ ) reaches a maximum value of  $2^2/3^3 = 4/27$  when  $R_A = 2R_B$ . As a consequence, we have the general inequality

$$\epsilon_A^{\text{contact}} \leq \frac{4}{27} \frac{c_B}{c_A}. \quad (77)$$

In the present case,  $B$  denotes a BH (with  $c_B = \frac{1}{2}$ ) so that  $\epsilon_A^{\text{contact}} \leq 2/(27c_A) = 0.074074/c_A$ . Upon multiplication by  $h_2^A \sim 0.8$  this yields  $h_2^A \epsilon_A^{\text{contact}} \lesssim 0.06/c_A$ . As NS compactnesses are expected to be larger than about 0.13, we find that the NS in a BHNS system is expected to be always deformed by less than 50% up to the moment of “contact” with its BH companion. Actually, the reasoning above shows that such large deformations are only attained when  $R_A = 2R_B$ , i.e. when the mass ratio is equal to

$$\frac{M_B}{M_A} = \frac{c_B}{c_A} \frac{R_B}{R_A} = \frac{1}{2} \frac{c_B}{c_A} = \frac{1}{4c_A}. \quad (78)$$

For typical NS compactnesses  $c_A \sim 0.15$ , such a mass ratio  $M_B/M_A \sim 1.67$  would correspond to a BH of a small mass ( $M_B \sim 2.3 M_\odot$ ). Larger BH masses will lead to smaller deformations of the NS.

Summarizing, the main conclusions of this subsection are that: (i) the EOB formalism predicts that the “quasi point mass” description can be applied up to contact, without the possibility of a disruption of the NS's in a well detached state, and (ii) the divide between the systems that undergo a plunge before contact and those that don't depend strongly both on the compactness and on currently unknown higher PN corrections to tidal effects.

To end this subsection, let us mention that our results are *robust* under the choice of the EOB parameters  $a_5$  and  $a_6$  entering the BBH radial  $A^0(r)$  potential, Eq. (21). The comparison between the currently most sophisticated version of the EOB formalism and the most accurate numerical relativity simulations has constrained the couple of parameters ( $a_5, a_6$ ) to lie within a rather thin banana-like region in the  $(a_5, a_6)$  plane. We have checked that the results that we present in this paper are quite insensitive to the choice of  $a_5$  and  $a_6$  within this “good” region. The default values that we use in the present paper are  $a_5 = -6.37$ ,  $a_6 = +50$ , which lie in the “good” region. To illustrate the insensitivity of our results to this choice, let us mention that the value of twice the orbital frequency at LSO,  $2M\Omega_{\text{LSO}}^{\text{EOB}}(a_5, a_6)$  (for an equal mass BNS system and for  $c = 0.17$ ), changes from the value 0.13605, quoted in Table III, to the new value 0.13603 for  $a_5 = -4$  and  $a_6 = 24$  which lie near the upper boundary of the good region of parameters discussed in Ref. [1].

TABLE III: Adiabatic LSO information for BNS and BBH systems. The NS models are built using the piece-wise polytropic SLy EOS. From left to right, the columns report: the composition of the binary, the compactness  $c$  of the objects, the NS mass  $M$ , the NS radius  $R$ , twice the orbital frequency at the adiabatic (EOB) LSO  $2GM\Omega_{\text{LSO}}^{\text{adiab}}$ , the corresponding LSO radius  $r^{\text{contact}}/GM$ , the “contact” frequency  $2GM\Omega^{\text{contact}}$  and the corresponding radial distance  $r^{\text{contact}}/GM$ .

System	$c$	$M [M_{\odot}]$	$R [\text{km}]$	$2GM\Omega_{\text{LSO}}^{\text{adiab}}$	$r_{\text{LSO}}/GM$	$2GM\Omega^{\text{contact}}$	$r^{\text{contact}}/GM$
BNS <sup>LO</sup>	0.13	1.0050	11.417	0.10208	7.3991	0.09590	7.6923
BNS <sup>LO</sup>	0.17	1.3205	11.470	0.13605	6.0111	0.14060	5.8824
BNS <sup>LO</sup>	0.17385	1.35	11.466	0.13902	5.9163	0.145061	5.7521
BNS <sup>NLO</sup> <sub><math>\alpha_1=7.0</math></sub>	0.13	1.0050	11.417	0.09056	8.1698	0.09834	7.6923
BNS <sup>NLO</sup> <sub><math>\alpha_1=7.0</math></sub>	0.17385	1.35	11.466	0.12185	6.5120	0.148750	5.7521
BBH <sub><math>\nu=1/4</math></sub>	0.5	...	...	0.19285	4.6186	...	...
BBH <sub><math>\nu=0</math></sub>	0.5	...	...	0.13608	6.0000	...	...

### B. Phasing and waveform from the non-adiabatic inspiral of tidally interacting compact binaries

Let us now consider the motion and radiation of tidally interacting binaries predicted by the full EOB formalism, i.e. beyond the adiabatic approximation. This is obtained by integrating the EOB equations of motion

$$\begin{aligned}
 \frac{dr}{dt} &= a(r) \frac{\partial \hat{H}_{\text{EOB}}}{\partial p_{r_*}}, \\
 \frac{dp_{r_*}}{dt} &= -a(r) \frac{\partial \hat{H}_{\text{EOB}}}{\partial r}, \\
 \frac{d\varphi}{dt} &= \frac{\partial \hat{H}_{\text{EOB}}}{\partial p_{\varphi}}, \\
 \frac{dp_{\varphi}}{dt} &= \hat{\mathcal{F}}_{\varphi},
 \end{aligned} \tag{79}$$

where  $a(r) \equiv AD^{-1/2}$ ,  $\hat{H}_{\text{EOB}}(r, p_{r_*}, p_{\varphi}) \equiv H_{\text{EOB}}/\mu$ , with  $H_{\text{EOB}}$  defined by Eq. (18) above, and where the (scaled) radiation reaction  $\hat{\mathcal{F}}_{\varphi} = \mathcal{F}_{\varphi}/\mu$  is defined in the way introduced in [13] improved (see Eq. (3) there), i.e. by summing over  $\ell$  and  $m$  the adiabatic multipolar partial fluxes corresponding to the newly resummed multipolar waves  $h_{\ell m}$  (including the tidal correction (68) in  $h_{22}$ ). In addition, we recall that  $r \equiv R/GM$ ,  $t \equiv T/GM$ ,  $p_{\varphi} \equiv P_{\varphi}/GM\mu$ , and that the function  $A(r)$  is here defined as the sum (22). Concerning the other metric coefficient  $D^{-1}(r)$  (entering the auxiliary function  $a \equiv (A/B)^{1/2} \equiv AD^{-1/2}$ ) we replace it by its standard resummation ( $u \equiv 1/r$ )

$$D^{-1}(r) = 1 + 6\nu u^2 + 2(26 - 3\nu)\nu u^3. \tag{80}$$

The solution of the ODE’s (79) is then inserted in the newly resummed (and tidally completed) multipolar

waves  $h_{\ell m}$  to compute the waveform emitted by the inspiralling compact binary. Here, we shall focus on the  $\ell = 2$ ,  $m = 2$  dominant asymptotic waveform  $\lim_{R \rightarrow \infty} (R h_{22})$ . Scaling it by  $G\mu \equiv GM\nu$  and decomposing it in amplitude and phase,

$$\frac{R}{GM} \frac{h_{22}}{\nu} = A_{22}(t) e^{-i\phi_{22}(t)}, \tag{81}$$

we can then consider the dominant “metric” gravitational wave frequency  $\omega_{22}(t) \equiv d\phi_{22}(t)/dt$ . [Note that all these quantities are dimensionless. In particular  $\omega_{22} \equiv GM\omega_{22}^{\text{phys}}$ .]

Up to now we have discussed an extension of the EOB formalism which incorporates tidal effects in both the motion and the radiation of compact binaries. However, it has been advocated [10, 12, 40] to incorporate tidal effects as a modification of one of the non-resummed “post-Newtonian”-based ways of describing the dynamics of inspiralling binaries. In particular, the recent Ref. [12] uses as baseline a time-domain T4-type incorporation of tidal effects. To be precise, let us recall that the phasing of the T4 approximant is defined by the following ODEs

$$\begin{aligned}
 \frac{d\phi_{22}^{\text{T4}}}{dt} &= 2x^{3/2}, \\
 \frac{dx}{dt} &= \frac{64}{5}\nu x^5 \left\{ a_{3.5}^{\text{Taylor}}(x) + a^{\text{tidal}}(x) \right\}
 \end{aligned} \tag{82}$$

where  $a_{3.5}^{\text{Taylor}}$  is the PN expanded expression describing point-mass contributions, and where  $a^{\text{tidal}}$  is given in the equal mass case by [10]

$$a^{\text{tidal}}(x) = 26\kappa_2^{\text{T}} x^5. \tag{83}$$

Here we shall analyze the (metric) GW phase  $\phi_{22}$  as a function of the corresponding dimensionless frequency  $\omega_{22}$  and study the influence on it of tidal effects. More precisely, we give here two different comparisons between the EOB predictions and the T4 one. In these two comparisons, we keep T4 unchanged and defined by

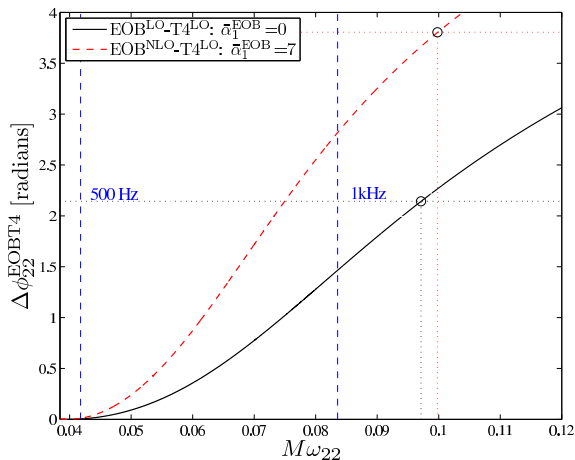


FIG. 5: Accumulated GW phase difference (versus GW frequency  $\omega_{22}$ ) between tidal-EOB (quadrupolar) waveforms and a Taylor-T4-based PN waveform with (leading order) tidal corrections, Eq. (82). Waveforms have been suitably aligned (subtracting a relative time and phase shift) at low frequencies. The circles on the plot indicate, for each curve, the dephasing accumulated up to the “contact” frequencies.

Eq. (82), with a tidal contribution of the *leading order* (LO) type (83). On the other hand, we compare this tidal-T4 model to two different tidal-EOB models; both models use a tidally modified  $A$  function, Eq. (22). One model (EOB<sup>LO</sup>) uses the LO  $A^{\text{tidal}}$ , Eq. (23), while the other one (EOB<sup>NLO</sup>) uses the *Taylor* NLO  $A^{\text{tidal}}$ , Eq. (39), with  $\bar{\alpha}_1 = 7$ . Here we consider a BNS equal-mass system modelled using the 2H EOS with compactness  $c = 0.13097$ , mass  $M = 1.35M_\odot$  and radius  $R = 15.23$  km.

The quantity which is plotted in Fig. 5 is the difference  $\Delta\phi_{22}^{\text{EOBT4}}(\omega_{22}) \equiv \phi_{22}^{\text{EOB}^X}(\omega_{22}) - \phi_{22}^{\text{T4}}(\omega_{22})$ , where the label X on EOB takes two values, X=LO for the leading order model and X=NLO for the next-to-leading order model. To compute this quantity we took into account possible shifts in both  $t$  ( $t^{\text{T4}} = t^{\text{EOB}} + \tau$ ) and  $\phi$  ( $\phi^{\text{T4}} = \phi^{\text{EOB}} + \alpha$ ). We use here the “two-frequency pinching” technique of Ref. [44] to fix suitable values of the shifts  $\tau$  and  $\alpha$ . We use here two pinching frequencies which are close to 450 Hz. In other words, the phase differences displayed in our figure show the phase differences accumulated for frequencies between 450 Hz and the contact. Though, the figure does not display the phase differences below 450 Hz we have checked that they remain much smaller than what they become for frequencies higher than 450 Hz.

In Fig. 5, the solid line (black online) displays  $\Delta\phi_{22}^{\text{EOBT4}}(\omega_{22}) = \phi_{22}^{\text{EOB}^{\text{LO}}}(\omega_{22}) - \phi_{22}^{\text{T4}}(\omega_{22})$ , and the dashed line (red online)  $\Delta\phi_{22}^{\text{EOBT4}}(\omega_{22}) = \phi_{22}^{\text{EOB}^{\text{NLO}}}(\omega_{22}) - \phi_{22}^{\text{T4}}(\omega_{22})$ . The two circles on the curves indicate the final moments of “contact”. We added two vertical (dashed) lines corresponding to 500 Hz and 1 kHz.

The main messages that one can draw from this figure are: i) the relative dephasing between EOB and T4 (using the same tidal model) grows by more than two radians up to contact; ii) the inclusion of higher-order PN tidal contributions further increases the relative dephasing by nearly two radians more. Note that even if one stops the evolution around 1 kHz (which is within the sensitivity of some possible configurations of Advanced LIGO) the previously discussed accumulated dephasings are still larger than one radian. This indicates that the GW phasing of the ultimate part of the BNS inspiral is very sensitive to tidal effects and also very sensitive to their precise analytical modelling, including higher-order PN corrections. This makes it urgent to do high-accuracy comparisons between accurate NR simulations of BNS inspiral and EOB models, so as to accurately “calibrate” the EOB description of higher-order PN tidal contributions.

## VII. CONCLUSIONS

We discussed an extension of the EOB formalism which includes tidal effects. The hope is that such a “tidal-EOB” formalism will be able to go beyond the present PN-based proposals whose validity is limited to the early (lower-frequency) portion of the GW inspiral signal emitted by BNS systems. This formalism allows naturally for the presence of higher-order PN corrections to the leading (Newtonian) effects. We compared tidal-EOB predictions to recently computed numerical relativity data of quasi-equilibrium circular BNS sequences [15]. We showed how to subtract tidal effects from NR data. Even after this subtraction, there remains a systematic difference between the “point-mass” NR binding energy and its EOB (and PN) analytical counterpart. We argue that this difference is due to unaccounted 3PN-level effects linked to the imperfect satisfaction of the helical Killing vector condition (which should be satisfied for physically waveless solutions). We advocate that new nonconformally flat simulations be performed for sequences of helical-Killing-vector cut-off radii so as to allow extrapolation to infinite radius. We also suggested to study BHNS circular binaries for mass ratios  $M_{\text{BH}}/M_{\text{NS}}$  of order unity.

In absence of such physically waveless NR data, we propose to subtract from the current data a term  $\delta x^4$  representing a 3PN correction in the binding energy. We could then do a least-square analysis to try to minimize the (squared) “distance”  $\chi^2$  between NR data and tidal-EOB predictions. Our analysis allowed for 1PN-corrections to tidal effects parametrized by  $\bar{\alpha}_1$ . We found that  $\chi^2$  remains close to its global minimum in a flat valley that extends over a significant region of the  $(\bar{\alpha}_1, \delta)$  plane. This means that, given the present error level in numerical data, we cannot meaningfully and simultaneously select preferred values for  $\bar{\alpha}_1$  and  $\delta$ . Though this analysis is not fully conclusive, it does suggest the need of including higher-order PN correction

to tidal effects that *significantly* increase their dynamical effect. [In other words, the “effective” value, say  $\kappa_2^{\text{eff}}(u) = \kappa_2^{\text{T}}(1 + \bar{\alpha}_1 u + \bar{\alpha}_2 u^2 + \dots)$ , which is relevant for the late inspiral is significantly larger, by a factor  $\sim 2$ , than  $\kappa_2^{\text{T}}$ ]. These higher-order PN corrections might come not from the 1PN level, but from higher PN levels (see in particular the end of Sec. IV, where a 2PN completion of a recently computed 1PN correction of order unity was shown to be fully compatible with current NR data).

This emphasizes the need both of higher order analytical calculations of tidal effects and of high-accuracy numerical relativity simulations of inspiralling BNS systems.[We note in this respect that it would be useful to refine the piece-wise polytropic approximation to realistic tabulated EOS (used in this paper) by incorporating the relativistic Love numbers, notably  $k_2$ , within the set of observables that are fitted]. We argued that such a suitably tidally completed EOB formalism will be able to describe the dynamics (and GW emission) of inspiralling BNS systems essentially up to the contact of the two neutron stars. We emphasized that, though below the dimensionless (quadrupolar) GW frequency  $GM\omega_{22} \sim 0.04$  (which corresponds to a frequency of 480 Hz for  $1.35M_\odot + 1.35M_\odot$  system) the present analytical knowledge is possibly sufficient for accurately describing the system, the GW phasing becomes uncertain

by a large amount ( $\sim 4$  radians) during the late part of the inspiral, because of our current lack of secure knowledge of higher order PN corrections to tidal effects. This makes it urgent to do high-accuracy comparisons between accurate NR simulation of BNS inspiral and EOB models. When the EOB description of higher-PN tidal effects is “calibrated” with sufficient accuracy by using such EOB/NR comparisons, we think it will be possible to use the EOB formalism to extract from Advanced-LIGO data some accurate knowledge of the nuclear EOS (via the measurement of the crucial parameter  $\kappa_2^{\text{T}}$ ).

### Acknowledgments

We are grateful to Loïc Villain for collaboration, at an early stage, on the NR-EOB comparison. We thank Koji Uryū for making available to us the numerical data behind the published tables of Ref. [15]. We are also grateful to Luca Baiotti, Bruno Giacomazzo and Luciano Rezzolla for sharing with us, before publication, their data on inspiralling and coalescing binary neutron stars, which prompted our interest in relativistic tidal properties of neutron stars.

- 
- [1] T. Damour and A. Nagar, Phys. Rev. D **79**, 081503 (2009) [arXiv:0902.0136 [gr-qc]].
- [2] A. Buonanno, Y. Pan, H. P. Pfeiffer, M. A. Scheel, L. T. Buchman and L. E. Kidder, Phys. Rev. D **79**, 124028 (2009) [arXiv:0902.0790 [gr-qc]].
- [3] N. Yunes, A. Buonanno, S. A. Hughes, M. C. Miller and Y. Pan, arXiv:0909.4263 [gr-qc].
- [4] L. Baiotti, B. Giacomazzo and L. Rezzolla, Class. Quant. Grav. **26**, 114005 (2009) [arXiv:0901.4955 [gr-qc]].
- [5] B. Giacomazzo, L. Rezzolla and L. Baiotti, Mon. Not. Roy. Astron. Soc. **399**, L164 (2009) [arXiv:0901.2722 [gr-qc]].
- [6] L. Baiotti, B. Giacomazzo and L. Rezzolla, Phys. Rev. D **78**, 084033 (2008) [arXiv:0804.0594 [gr-qc]].
- [7] L. Bildsten and C. Cutler, Astrophys. J. **400**, 175 (1992).
- [8] C. S. Kochanek, Astrophys. J. **398**, 234 (1992).
- [9] M. Vallisneri, Phys. Rev. Lett. **84**, 3519 (2000) [arXiv:gr-qc/9912026].
- [10] E. E. Flanagan and T. Hinderer, Phys. Rev. D **77**, 021502 (2008) [arXiv:0709.1915 [astro-ph]].
- [11] T. Hinderer, Astrophys. J. **677**, 1216 (2008) [arXiv:0711.2420 [astro-ph]].
- [12] T. Hinderer, B. D. Lackey, R. N. Lang and J. S. Read, arXiv:0911.3535 [astro-ph.HE].
- [13] T. Damour and A. Nagar, Phys. Rev. D **80**, 084035 (2009) [arXiv:0906.0096 [gr-qc]].
- [14] T. Binnington and E. Poisson, Phys. Rev. D **80**, 084018 (2009) [arXiv:0906.1366 [gr-qc]].
- [15] K. Uryū, F. Limousin, J. L. Friedman, E. Gourgoulhon and M. Shibata, arXiv:0908.0579 [gr-qc].
- [16] K. Uryū, F. Limousin, J. L. Friedman, E. Gourgoulhon and M. Shibata, Phys. Rev. Lett. **97**, 171101 (2006) [arXiv:gr-qc/0511136].
- [17] T. Damour, C. R. Acad. Sc. Paris, Série A, **291**, 227 (1980).
- [18] T. Damour, in *Gravitational Radiation*, edited by N. Deruelle and T. Piran (North-Holland, Amsterdam, 1983), p.59;
- [19] T. Damour, P. Jaranowski and G. Schaefer, Phys. Lett. B **513**, 147 (2001) [arXiv:gr-qc/0105038].
- [20] L. Blanchet, T. Damour and G. Esposito-Farese, Phys. Rev. D **69**, 124007 (2004) [arXiv:gr-qc/0311052].
- [21] L. Blanchet, T. Damour, G. Esposito-Farese and B. R. Iyer, Phys. Rev. Lett. **93**, 091101 (2004) [arXiv:gr-qc/0406012].
- [22] T. Damour and G. Esposito-Farese, Phys. Rev. D **53**, 5541 (1996) [arXiv:gr-qc/9506063].
- [23] W. D. Goldberger and I. Z. Rothstein, Phys. Rev. D **73**, 104029 (2006) [arXiv:hep-th/0409156].
- [24] T. Damour and G. Esposito-Farese, Phys. Rev. D **58**, 042001 (1998) [arXiv:gr-qc/9803031].
- [25] T. Damour, M. Soffel and C. m. Xu, Phys. Rev. D **43**, 3272 (1991).
- [26] T. Damour, arXiv:0910.5533 [gr-qc].
- [27] L. Blanchet and T. Damour, Phil. Trans. R. Soc. Lond. A, **320**, 379 (1986).
- [28] T. Damour, M. Soffel and C. m. Xu, Phys. Rev. D **45**, 1017 (1992).
- [29] T. Damour and G. Esposito-Farèse, in preparation
- [30] T. Damour, M. Soffel and C. m. Xu, Phys. Rev. D **47**, 3124 (1993).
- [31] T. Damour, M. Soffel and C. m. Xu, Phys. Rev. D **49**,

- 618 (1994).
- [32] A. Buonanno and T. Damour, Phys. Rev. D **59**, 084006 (1999) [arXiv:gr-qc/9811091].
- [33] A. Buonanno and T. Damour, Phys. Rev. D **62**, 064015 (2000) [arXiv:gr-qc/0001013].
- [34] T. Damour, Phys. Rev. D **64**, 124013 (2001) [arXiv:gr-qc/0103018].
- [35] T. Damour, P. Jaranowski and G. Schafer, Phys. Rev. D **62**, 084011 (2000) [arXiv:gr-qc/0005034].
- [36] T. Damour and A. Nagar, arXiv:0906.1769 [gr-qc].
- [37] T. Mora and C. M. Will, Phys. Rev. D **69**, 104021 (2004) [Erratum-ibid. D **71**, 129901 (2005)] [arXiv:gr-qc/0312082].
- [38] T. Damour, P. Jaranowski and G. Schafer, Phys. Rev. D **62**, 044024 (2000) [arXiv:gr-qc/9912092].
- [39] J. S. Read, B. D. Lackey, B. J. Owen and J. L. Friedman, Phys. Rev. D **79**, 124032 (2009) [arXiv:0812.2163 [astro-ph]].
- [40] J. S. Read, C. Markakis, M. Shibata, K. Uryū, J. D. E. Creighton and J. L. Friedman, Phys. Rev. D **79**, 124033 (2009) [arXiv:0901.3258 [gr-qc]].
- [41] P. Jaranowski and G. Schafer, Phys. Rev. D **57**, 7274 (1998) [Erratum-ibid. D **63**, 029902 (2001)] [arXiv:gr-qc/9712075].
- [42] T. Damour, B. R. Iyer and A. Nagar, Phys. Rev. D **79**, 064004 (2009) [arXiv:0811.2069 [gr-qc]].
- [43] T. Damour and A. Gopakumar, Phys. Rev. D **73**, 124006 (2006) [arXiv:gr-qc/0602117].
- [44] T. Damour, A. Nagar, E. N. Dorband, D. Pollney and L. Rezzolla, Phys. Rev. D **77**, 084017 (2008) [arXiv:0712.3003 [gr-qc]].
- [45] T. Damour and A. Nagar, Phys. Rev. D **77**, 024043 (2008) [arXiv:0711.2628 [gr-qc]].